International Journal of Nanomedicine

Dovepress
open access to scientific and medical research

Open Access Full Text Article

ORIGINAL RESEARCH

Dual-mRNA Delivery Using Tumor Cell Lysate-Based Multifunctional Nanoparticles as an Efficient Colon Cancer Immunogene Therapy

Kaiyu Wang[1,*], Yan Gao[1,*], Shan Wu[1,*], Jin Zhang[1], Manfang Zhu[2], Xiayu Chen[1], Xizi Fu[1], Xingmei Duan[2], Ke Men[1]

[1]State Key Laboratory of Biotherapy and Cancer Center, West China Hospital, Sichuan University, Chengdu, 610041, People's Republic of China; [2]Department of Pharmacy, Personalized Drug Therapy Key Laboratory of Sichuan Province, Sichuan Academy of Medical Sciences & Sichuan Provincial People's Hospital, School of Medicine, University of Electronic Science and Technology of China, Chengdu, 610072, People's Republic of China

*These authors contributed equally to this work

Correspondence: Xingmei Duan, Department of Pharmacy, Personalized Drug Therapy Key Laboratory of Sichuan Province, Sichuan Academy of Medical Sciences & Sichuan Provincial People's Hospital, School of Medicine, University of Electronic Science and Technology of China, Chengdu, 610072, People's Republic of China, Email duanxingmei2003@163.com; Ke Men, State Key Laboratory of Biotherapy and Cancer Center, West China Hospital of Sichuan University, Chengdu, 610041, People's Republic of China, Email mendingbob@hotmail.com

Background: Messenger RNA (mRNA)-based immunogene therapy holds significant promise as an emerging tumor therapy approach. However, the delivery efficiency of existing mRNA methods and their effectiveness in stimulating anti-tumor immune responses require further enhancement. Tumor cell lysates containing tumor-specific antigens and biomarkers can trigger a stronger immune response to tumors. In addition, strategies involving multiple gene therapies offer potential optimization paths for tumor gene treatments.

Methods: Based on the previously developed ideal mRNA delivery system called DOTAP-mPEG-PCL (DMP), which was formed through the self-assembly of 1.2-dioleoyl-3-trimethylammonium-propane (DOTAP) and methoxypoly (ethylene glycol)-b-poly (ε-caprolactone) (mPEG-PCL), we introduced a fused cell-penetrating peptide (fCPP) into the framework and encapsulated tumor cell lysates to form a novel nanovector, termed CLSV system (CLS: CT26 tumor cell lysate, V: nanovector). This system served a dual purpose of facilitating the delivery of two mRNAs and enhancing tumor immunogene therapy through tumor cell lysates.

Results: The synthesized CLSV system had an average size of 241.17 nm and a potential of 39.53 mV. The CLSV system could not only encapsulate tumor cell lysates, but also deliver two mRNAs to tumor cells simultaneously, with a transfection efficiency of up to 60%. The CLSV system effectively activated the immune system such as dendritic cells to mature and activate, leading to an anti-tumor immune response. By loading Bim-encoded mRNA and IL-23A-encoded mRNA, CLSV/Bim and CLSV/IL-23A complexes were formed, respectively, to further induce apoptosis and anti-tumor immunity. The prepared CLSV/dual-mRNA complex showed significant anti-cancer effects in multiple CT26 mouse models.

Conclusion: Our results suggest that the prepared CLSV system is an ideal delivery system for dual-mRNA immunogene therapy.

Keywords: mRNA gene therapy, dual-mRNA delivery, tumor cell lysates, Bim and IL-23A mRNAs, immune response

Introduction

Cancer has become a significant public health concern worldwide, with increasing mortality rates in many countries.[1] Traditional treatment approaches include surgery, radiation therapy, hormone therapy, chemotherapy, and targeted therapy (including immunotherapy), among others.[2] Among the promising novel strategies, messenger RNA (mRNA) gene therapy has emerged as a cutting-edge approach, involving utilizing synthetic mRNA molecules to convey genetic instructions to cells.[3,4] On the basis of its non-integrative, rapid expression, and biodegradable characteristics, the potential of mRNA gene therapy for disease treatment has been widely acknowledged.[5] For instance, during the 2019 coronavirus disease pandemic, two mRNA vaccines (BNT162b2 and mRNA-1273) were the first to receive emergency

Received: 30 November 2023
Accepted: 27 April 2024
Published: 27 May 2024

approval.[6,7] Because cancer is a complex disease associated with multiple inherited genes, single-gene targeted therapy can have limited therapeutic effects;[8] therefore, exploring the potential of dual-mRNA gene therapy has the potential to transform treatment strategies and further improve the therapeutic effect.

The dual-mRNA gene therapy approach, which allows simultaneous delivery of two functional mRNAs, has many advantages in cancer treatment. This approach can express proteins encoded by two therapeutic genes, thereby exerting two or more anti-tumor therapeutic strategies. These two mRNAs can cooperate to achieve complementary or superimposed anti-tumor effects, which can simultaneously mediate killing or intervention effects inside or outside tumor cells.[9] In addition, dual-mRNA gene therapy ensures that even if the effect of the action of one mRNA is diminished, the other mRNA can still perform its function, thus amplifying the overall enhancement of the anti-tumor effect. However, there are some challenges in efficiently co-delivering two mRNAs to the same target cells. First, mRNA itself is a linear molecule with a single chain that is irregularly folded, has poor stability, and is easily degraded by enzymes.[10] In addition, double mRNA molecules have different lengths and folding forms, which make them difficult to compress with the same carrier. The folding exposure of the two mRNAs is also different, so it is difficult to protect both mRNAs from degradation and maintain stability with the same vector. Additionally, ensuring that the two mRNAs are delivered to the same cell to perform their respective functions requires a vector with highly efficient delivery capability. Therefore, it is necessary to develop non-viral gene vectors capable of efficiently delivering double mRNA molecules.

Improving mRNA delivery efficiency is the key to achieving the expected efficacy of dual-mRNA complexes. An effective strategy involves peptide modification, particularly using cell-penetrating peptides (CPPs), which are known for their high penetrative capabilities.[11] CPPs are short peptides that can traverse cell membranes and facilitate the transportation of various bioactive substances with differing sizes and properties into cells.[12] These peptides achieve cell membrane penetration through various mechanisms, including direct translocation or endocytosis, thereby enabling efficient delivery of cargo into the cytoplasm.[13] The ease of synthesis and functionalization of CPPs allows them to be readily incorporated into carriers through both non-covalent and covalent methods.[14] Despite these promising characteristics, coupling CPPs with nanomaterials remains a challenge. First, it is worth studying whether the modification of CPPs can affect the delivery efficiency of existing mRNA. In addition, there is a need to explore whether CPPs can effectively improve the delivery and uptake capacity of mRNA based on its characteristics. In addition, it is still necessary to investigate whether this modification can promote mRNA stability or even meet the need to promote efficient delivery of double mRNA molecules.

To further improve the efficacy of mRNA gene therapy, a combination of immunotherapy approaches can enrich and support tumor treatment strategies based on mRNA gene therapy. Cells, as natural immune stimulators, have immune properties due to the presence of various molecules and structures on their surface, including phospholipids, proteins, and polysaccharides, which can interact with components of the immune system.[15,16] As a unique cell population, tumor cells produce many new neoantigenic determinants due to gene mutations.[17] These neoantigenic determinants are expressed in large quantities on the membrane or in the cell and can be targeted by the immune system with strong immunogenicity.[18] In the pursuit of therapeutic applications, the use of intact tumor cells requires preservation of their vitality and structural integrity to play an immunostimulating role, which is both difficult and costly to prepare. Therefore, tumor cell lysates have great application prospects as a new strategy to replace tumor cells.[19,20] First, tumor cell lysates do not need to maintain cell activity and can fully retain the immunogenicity of tumor cells even in an inactivated state. Second, tumor cell lysates can release intracellular antigens, such as intracellular proteins or nucleic acids, which are more immunogenic than tumor cells.[21] Additionally, the tumor cell lysate is used in the form of a solution mixture, the dosage of which can be effectively controlled. However, there are many challenges to co-delivery of tumor cell lysates with mRNA. First, the tumor cell lysate is a mixture that cannot be delivered simply through electrostatic adsorption, but instead, it requires to be effectively wrapped by the carrier in addition to electrostatic adsorption. In addition, the composition of tumor cell lysates is complex, with different solubility, charge intensity, osmotic pressure, etc., which requires the delivery carrier to wrap the effective components as much as possible. In addition, even after the tumor cell lysate is wrapped into the carrier, the carrier must release it stably to achieve the purpose of immune stimulation. Therefore, choosing a suitable non-viral delivery vector is crucial to ensure that it can efficiently carry tumor lysates while still effectively delivering its mRNA cargo.

In our previous research, we successfully constructed ideal mRNA delivery nanomicelles (DOTAP-mPEG-PCL, DMP) with high modifiability, biocompatibility, and safety.[22,23] In this study, based on the favorable characteristics of

DMP, we constructed a fused CPP (fCPP) by maleimide-thiol Michael reaction to conjugate to the DMP backbone and simultaneously encapsulated CT26 tumor lysate to form a novel nanovector, termed CLSV system (CLS: CT26 tumor cell lysate, V: nanovector). We hypothesized that the CLSV system could achieve the dual purpose of simultaneous delivery of two functional mRNAs and consequent immune system activation. Regarding the selection of the two mRNAs, we chose Bim and IL-23A mRNAs to co-deliver to tumor cells. Bim is an important member of the Bcl-2 protein family, which can induce tumor cell apoptosis, while IL-23A belongs to the IL-12 cytokine family and can trigger immune system activation in combination with CT26 tumor lysate.[24,25] Herein, the properties and dual-mRNA delivery capacity of the CLSV system are characterized in detail, and the therapeutic potential of CLSV/dual-mRNA complexes for colon cancer is further investigated.

Materials and Methods

Preparation and Characterization of Nanoparticles

To obtain CT26 cell lysates, we digested CT26 cells (purchased from American type culture collection (ATCC)) with trypsin, washed the cultured CT26 cells with dulbecco's phosphate-buffered saline (DPBS) three times, and prepared a cell suspension at 1×10^7 cells/mL. Subsequently, the harvested cells were oxidatively lysed with hypochlorous acid (6.42×10^{-1}/mL). The CT26 cell lysates were obtained by repeated freezing and thawing (14–16 times) and sonicating the cell suspension for 30 min (10 s each time, with a 1-min interval). Finally, the protein concentration in the lysate was determined using the BCA method (Thermo, California, USA).

The CLSV system was synthesized on the basis of the cationic nanoparticles (DMP) obtained by our research group.[23,26] Briefly, N-[1-(2,3-dioleoyloxy) propyl]-N, N, N-trimethylammonium methyl-sulfate (cationic lipid DOTAP, Avanti) and mPEG-PCL polymer (Ruixibio, China) (1:9, w/w) were co-dissolved in methylene dichloride. After removing the dichloromethane by rotary evaporation for 45 min, a uniform lipid film formed on the walls of the flask. Subsequently, the linker maleimide-PEG-PCL was added, and finally, the CT26 cell lysate was added to the flask for rehydration and self-assembly into maleimide-activated nanoparticles (DMP-mal-CT26 lysate). Then, a fused CPP (fCPP), which was the fused TAT-iRGD peptides (CRGDKGPDC-GRKKRRQRRRC, Shanghai APeptide, China), was dissolved in 2-[4-(2-hydroxyethyl)-1-piperazinyl] ethanesulfonic acid (HEPES, 50 mM) buffer and DMP-mal-CT26 lysate (1: 30, w/w), and reacted overnight at 4°C to obtain nanoparticles (CLSV) at a final concentration of 7.75 mg/mL. The prepared CLSV was stored at 4°C for future use. The particle size and zeta potential of the CLSV nanoparticles were measured by dynamic light scattering (Nano ZS, Malvern Panalytical, Malvern, UK), and the morphology was observed by transmission electron microscopy (TEM) (Tecnai G2 F20 S-TWIN, FEI, USA). All results are the average of three test runs.

CT26 Cell Lysates Encapsulation Efficiency and Loading Capacity

We used BCA method to determine the initial concentration and the concentration after loading, and calculated the encapsulation efficiency (EE) and loading capacity (LC) values of CT26 cell lysate in CLSV system. Briefly, we established the different concentration curve of standard BCA reagent and then added the initial CT26 cell lysates and the prepared CLSV to detect the light adsorption value under 562 nm. The encapsulation efficiency was calculated as

$$\mathrm{EE\%} = \frac{\mathrm{CT26\,cell\,lysate_{encapsulated}}}{\mathrm{CT26\,cell\,lysate_{total}}} \times 100\%$$

and drug loading capacity was calculated as

$$\mathrm{LC\%} = \frac{\mathrm{CT26\,cell\,lysate_{encapsulated}}}{\mathrm{materials}} \times 100\%$$

The Binding Efficiency of fCPP Conjugated to DMP-Mal-Lysate

The binding efficiency of fCPP was obtained by indirectly measuring the content of fCPP in the dialysate, which was collected and frozen-dried after the overnight dialysis of prepared CLSV solution in ultra-pure water at 4 °C using Slide-A-Lyzer dialysis cassette (3500 MWCO, Thermo, USA). The concentration of fCPP in the dialysate was quantified by

the valid RP-HPLC method with Agilent 1260 Infinity II LC system (Agilent Technologies, USA). The analytic process was performed on a ZORBAX StableBond 300 C18 column (5 μm, 4.6×150 mm) and the mobile phase contained a mixture of solvent A (0.1% trifluoroacetic acid in water) and solvent B (0.1% trifluoroacetic acid in acetonitrile) gradient varied from 95/5 (v/v) to 10/90 (v/v) in 18 min at a flow rate of 1 mL / min. The sample volume was 10 μL and the UV detector wavelength was 214 nm. The binding efficiency was equal to the proportion of fCPP in the dialysate to the feeding amount of fCPP in the reaction with DMP-mal CT26 lysate using the formula:

$$\text{Conjugation efficiency\%} = \frac{\text{Total}_{\text{fcpp}} - \text{Measured}_{\text{fcpp}}}{\text{Total}_{\text{fcpp}}} \times 100\%$$

Thermogravimetric Analysis (TGA) and Fourier-Transform Infrared Spectroscopy (FTIR) Spectra

The TGA analysis was carried out by using a TGA/SDTA 851 Mettler Toledo thermobalance, under controlled nitrogen atmosphere between 30 °C and 600 °C at a heating rate of 10 °C/min. Three samples were analyzed: (a) DMP; (b) CLSV before purification; (c) CLSV after a purification step to ensure the removal of reactants.

To further investigated the successful formation of the CLSV, we used Nicolet Nexus 670 FITR (Thermo Electron Corporation, USA) to characterize CLSV. The spectra were obtained at wavenumbers between 400 and 4000 $cm^{-1}$and a resolution of 0.16 cm^{-1}.

The Stability of CLSV in vitro

To assess in vitro the stability of prepared CLSV nanoparticles in normal saline to mimic in vivo condition, CLSV nanoparticles were incubated in normal saline at 37 °C for different time (0 h, 4 h, 8 h, 24 h, 48 h,72 h,96 h). The size of each sample on various time was measured by dynamic light scattering (Nano ZS, Malvern Panalytical, Malvern, UK).

CLSV Whether Can Release CT26 Cell Lysates in vitro

We employed the BCA method to monitor the release of protein mass from CLSV. In a 24-well plate, 500 μL of phosphate-buffered saline (PBS) was added to each well, and 300 μL of C26 cell lysate and CLSV from the same batch were added to separate wells. Samples of 25 μL were taken from each well at 0, 1, 2, 4, 6, 8, 12, 18, and 24 hours. To these samples, 200 μL of BCA working solution was added, mixed for 30 seconds, and then incubated at 37°C for 30 minutes. Subsequently, the solution was cooled to room temperature, and absorbance at 562 nm was measured. A standard curve for protein concentration was constructed using different concentrations of standard protein solutions. The protein mass in each well was then calculated using the formula: $m = c \times v$.

In vitro mRNA Transcription

To obtain in vitro transcription (IVT) mRNA, we used the IVT method based on T7 polymerase. Initially, we used PVAX1-Bim plasmid DNA (pBim) as a PCR template to generate a linear IVT Bim template. The forward primer sequence for pBim was 5′-TAATACGACTCACTATAGG GAGAATGGCCAAGCAACCTTCT-3′, whereas the reverse primer sequence was 5′-ATGCCTTCTCCATAC CAGACG-3′. Similar to the above method, we used PVAX1-IL-23A plasmid DNA as a PCR template to generate a linear IVT IL-23A template (forward primer: 5′-TAATACGACTCACTATAGGGATGCTGGATTGC AGAGCAGT-3′; reverse primer: 5′-AGCTGTTGGCACTAAGGGCT-3′). Subsequently, mouse Bim mRNA (Bim) and IL-23A mRNA were synthesized with a 0.5 μg template using the mMESSAGE-mMACHINETM T7 transcription kit (Thermo, USA). After synthesis, the mRNA was purified using the MEGAclearTM Transcription Clean-Up Kit (Thermo, USA) following the manufacturer's instructions. To ensure the integrity of the mRNA, we analyzed it on agarose gel and confirmed its full-length properties.

mRNA Gel Retardation Assay

To assess the binding ability of CLSV nanoparticles with mRNA, different molecular ratios of CLSV nanoparticles were mixed with Bim (0.5 μg) and electrophoresed on a 1% (w/v) agarose gel at 120 V for 15 min. When CLSV binds to

mRNA, the molecular weight increases, and migration in the gel is prevented, resulting in shortened bands. The gel was then stained with GoldView II Nuclear Staining Dye (Solarbio), and the bands were detected using an E-gel imager (Bio-Rad, ChemiDox XRS, USA).

RNase Protection Assay

To assess the protective ability of CLSV on mRNA against RNase A (Solarbio, Beijing), naked Bim or CLSV/Bim was exposed to RNase A at a final concentration of 0.25 mg/mL and incubated at 37°C for 0 min, 15 min, 1 h, 2 h, and 4 h. Subsequently, denaturation was achieved by adding sodium dodecyl sulfate (SDS) at a concentration of 0.24 mg/mL and heating at 70°C for 10 min. Finally, the samples were subjected to electrophoresis on a 1% (w/v) agarose gel for 15 min at 120 V.

Cytotoxicity Assay

Next, the MTT assay was used to assess the in vitro cytotoxicity of CLSV nanoparticles. Briefly, 293T cells ((purchased from American type culture collection (ATCC)) were plated in 96-well plates at a density of 5×10^3 cells per well and incubated overnight at 37°C. Once the desired cell density was reached, various concentrations of CLSV and DMP-CPPs were added to the wells, with PEI25K used as the standard control. After transfection for 24 h at 37°C, 20 μL of MTT solution was added to each well to halt the reaction, and the cells were further incubated for 4 h. Following incubation, the medium in each well was replaced with 150 μL of dimethyl sulfoxide, and the plates were further incubated at room temperature for 15 min with gentle shaking. Subsequently, the absorbance at 570 nm was measured using a Spectramax Absorbance Reader (Molecular Devices, USA), enabling the evaluation of CLSV nanoparticle cytotoxicity against 293T cells.

Pharmacokinetics Study

For the in vivo pharmacokinetics study, we first used mass spectrometer to establish standard curve different content of CLSV nanoparticles. Then female BALB/c mice (5–6 weeks) were intravenously administrated CLSV nanoparticles (7.75 mg/mL, 100 μL) and then detect the content of CLSV nanoparticles in mice blood through UFLC(SHIMADZU)-Qtrap 5500 Mass Spectrometer (AB SCIEX) in the following time:0 h, 0.25 h, 1 h, 2 h, 6 h, 24 h.

Quantitative Real-Time PCR

For quantitative real-time PCR (qRT–PCR), we first extracted the total RNA from CT26 cells transfected with CLSV/Bim (1 μg) (25:1, w/w) and CLSV/IL-23A (1 μg) (25:1, w/w) complexes to quantify the levels of Bim and IL-23A mRNAs. Total RNA was extracted from cells by FastPure Cell/Tissue Total RNA Isolation Kit (Vazyme, China) after transfected. The isolated mRNA was validated via gel electrophoresis, followed by conversion to cDNA using SuperScript II (Vazyme) as a template. The SYBR Green ER quantitative PCR SuperMix Universal kit (Vazyme) was used for cDNA analysis. To quantify the expression levels of Bim and IL-23A, mouse β-actin was chosen as a reference. The PCR primers for Bim (forward: 5′TTTGACA CAGACAGGAGCCC; reverse: 5′-CAGCTCCTGTGCAATCCGTA), IL-23A (forward: 5’-CCAGCGGGACATATG AATCTAC; reverse: 5′-GCTGTTGTCCTTGAGTCCTT), and β-actin (forward: 5′-CCCAGGCATTGCTGACAGG; reverse: 5′-TGGAAGGTGGACAGTGAGGC) were synthesized and purified.

In vitro Transfection of CLSV

The transfection efficiency of the CLSV/mRNA complex was assessed by flowcytometry. In brief, 293T and CT26 cells were seeded in 24-well plates (3×10^4 cells per well) and incubated overnight in a humidified atmosphere at 37°C under 5% CO_2. Subsequently, the cells in each well were transfected with the CLSV/mRNA (EGFP/mCherry mRNA, 0.5 μg/0.5 μg, 25:1, w/w) complex, and the medium was replaced with DMEM for expression. Four hours later, the medium was replaced with complete growth medium. Transfection controls, PEI25K/mRNA (EGFP/mCherry mRNA, 0.5 μg/0.5 μg, 1:1, w/w), DMP/mRNA (EGFP/mCherry mRNA, 0.5 μg/0.5 μg, 25:1, w/w), and DMP-CPPs/mRNA (EGFP/mCherry mRNA, 0.5 μg/0.5 μg, 25:1, w/w) were also used for comparison. After a 48-h incubation period, the cells were observed under a fluorescence microscope, and the transfection efficiency of the CLSV/mRNA complex was quantified by flow cytometry (NovoCyte Flow Cytometer, ACEA Biosciences, USA).

Cellular Uptake Mechanism of the CLSV/mRNA Complex

To determine the cellular uptake mechanism of the CLSV/mRNA complex, we treated CT26 (3×10^4 cells per well, 24 wells) with chlorpromazine (1 μg/mL), genistein (30 mM), wortmannin (10 mM), filipin III (1 mg/ mL) and methyl-β-cyclodextrin (10 mM) for 30 min before transfection. Forty-eight hours after transfection, we measured the transfection efficiency by flow cytometry. For fluorescence microscopy analysis, 2.5×10^4 cells were seeded in chamber slides (Millicell, 4 well-glass). Twenty-four hours later, CT26 cells were treated with various inhibitors using well-established protocols. After 48 h, the nuclei were stained with Hoechst (1 mg/mL, Solarbio), and the plasma membranes were stained with Dil (10 mg/mL, Beyotime). A fluorescence microscope (ZEN880, Bamboo Living) was used to capture and analyze the fluorescence emitted by different inhibitors.

Transfection Ability of CLSV Nanoparticles at Different Serum Concentrations in vitro

To investigate the stability of CLSV nanoparticles in serum, we evaluated transfection ability of CLSV nanoparticles at different serum concentrations in vitro. Briefly, CT26 cells (3×10^4 cells per well in 24-well plates) were transfected with the CLSV/EGFP mRNA (1 μg) (25:1, w/w) complex under different serum concentration (0%, 2%, 4%, 6%, 8%, 10%). After a 48-h incubation period, the cells were observed under a fluorescence microscope, and the transfection efficiency of the CLSV/EGFP mRNA complex was quantified by flow cytometry (NovoCyte Flow Cytometer, ACEA Biosciences, USA).

In vitro Immunostimulation Experiments

To demonstrate that CLSV can be taken up by antigen-presenting cells, we treated bone marrow-derived dendritic cells (BMDCs) with Cy5.5-labeled CLSV (200 μg) for 24 h. The nuclei were labeled with Hoechst and the cell membranes were labeled with Dio (CLSM, CLSM410, Zeiss, Germany). Then, a fluorescence microscope (ZEN880, Bamboo Living) was used to capture and analyze the Cy5.5-labeled CLSV uptake by dendritic cells (DCs).

Mouse DCs were extracted to evaluate the immunostimulatory effect of the prepared CLSV system in vitro. In brief, BMDCs were extracted from the hindlimb bones after dismemberment of BALB/c mice (female, 6–8 weeks) and cultured in RPMI 1640 medium containing 20 ng/mL GM-CSF (R&D, USA). On day 6, immature BMDCs were collected in six-well plates (6×10^5 BMDCs per well). On day 7, CT26 tumor cell lysate, DMP-CPPs, and CLSV (200 μg) (the quality of the DMP-CPPs and tumor cell lysate was the same as that of CLSV) were added to the well plate to immunologically stimulate immature BMDCs. Twenty-four hours later, the cells collected from each group were incubated with CD11C, CD80, CD86, and MHC-II antibodies (BioLegend, USA) at 4°C in the dark for 20 min. Subsequently, the cells were collected and washed with PBS for flow cytometry analysis (NovoCyte Flow Cytometer, ACEA Biosciences, USA).

In vivo Immunostimulation Experiments

To demonstrate the immunostimulatory effect of nanomaterials in vivo, CT26 tumor cell lysate, DMP-CPPs, and CLSV (200 μg) (DMP-CPPs and cell lysate were of the same quality as CLSV) were intramuscularly injected into BALB/c female mice at 6–8 weeks. After 24, 48, 72 h, the mice were sacrificed, and the inguinal lymph nodes and spleens were collected. Lymph nodes were punctured with the tip of a needle to release lymphocytes, and splenic lymphocytes were isolated using lymphocyte isolation medium (Dakewe, China). The lymphocytes were re-suspended in RPMI 1640 medium, centrifuged (1500 rpm, 5 min), washed with PBS, and harvested. DCs from each group were incubated with CD11C, CD80, CD86, and MHC-II antibodies (BioLegend, USA) at 4°C in the dark for 20 min. Subsequently, the cells were collected and washed with PBS for flow cytometry analysis (NovoCyte Flow Cytometer, ACEA Biosciences, USA).

Anti-Proliferation Assay

To assess the growth inhibition capacity of the Bim/CLSV complex, CT26 cells were seeded in a 96-well plate (1×10^3 cells per well) and incubated overnight at 37°C in a humidified atmosphere under 5% CO_2. CT26 cells were transfected with CLSV and CLSV/Bim (0.5 μg), following well-established protocols. After 96 h, the anti-proliferative activity was assessed using the MTT assay.

Clonogenic Assay

The clonogenic assay was used to assess the cell proliferation capacity of Bim/CLSV complex. In brief, CT26 cells were seeded in six-well plates at a density of 1×10^3 cells per well. After 24 h, the CT26 cells were transfected with CLSV and Bim (4 μg)/CLSV and cultured until the formation of colonies after 1–2 weeks. When the colonies became clearly visible to the naked eye, the supernatant was discarded, and the cells were gently rinsed twice with PBS. The colonies were then fixed with paraformaldehyde for 15 min and stained with crystal violet (0.1%) for at least 30 min. To determine the inhibition rate, the six-well plate was placed upside down on a transparent membrane, and colonies were counted.

In vitro Apoptosis Assay

To verify the apoptosis mechanism after Bim mRNA delivery, CLSV and CLSV/Bim (2 μg) were transfected into CT26 cells (3×10^4 cells per well, 24 wells). Forty-eight hours after transfection, cell samples from each group were collected, centrifuged, and re-suspended in Annexin V-fluorescein isothiocyanate (FITC) and propidium iodide staining solution (Genechem, Shanghai). The apoptosis rate was detected by flow cytometry.

Western Blotting

To study the relevant proteins in cells, CT26 cells (1×10^5 cells per well in six-well plates) were transfected with CLSV/Bim complex. After 48 h, the cells were collected, and the proteins were extracted using RIPA lysis buffer (Beyotime, China). To ensure consistent loading of protein samples, the total protein concentration was determined using Coomassie brilliant blue G-250 (Beyotime). Next, the proteins were separated by polyacrylamide gel electrophoresis (Beyotime) and transferred onto a polyvinylidene difluoride (PVDF) membrane (Millipore). The target protein was probed with Bim antibody (Abcam). Subsequently, the PVDF membrane was washed and then incubated with a goat-rabbit secondary antibody. Finally, the target proteins were detected using a chemiluminescence system (ChemiScope Touch, CLINX, Shanghai).

Detection of IL-23 Expression by Enzyme-Linked Immunosorbent Assay (ELISA)

The concentration of IL-23 in the cell culture supernatant was determined by ELISA. In brief, CT26 cells were pre-seeded into a six-well plate (1×10^4 cells per well). Subsequently, CLSV or CLSV/IL-23A (6 μg) was added to each well. After transfection for 96 h, the cell culture supernatant was collected and concentrated. The cytokine level was then measured using a mouse IL-23 ELISA Kit (Thermo), following the manufacturer's instructions.

In vitro Lymphocyte Stimulating Assay

To evaluate the proliferative effect of the secreted IL-23 on lymphocytes, we extracted splenic lymphocytes from 6–8-week-old BALB/c female mice. Initially, CT26 cells were transfected with CLSV or the CLSV/IL-23A (6 μg) complex for 96 h. The cell culture supernatant was then collected and concentrated, and the enriched supernatant was incubated with cultured lymphocytes derived from the mouse spleen. After 72 h, the splenic lymphocytes of each group were observed and counted. The activation of T cells and DCs was detected by flow cytometry.

Lymphocyte-Mediated Cytotoxicity Assay

To investigate the cytotoxic effects of stimulated lymphocytes on CT26 cells, cell culture supernatants from different CT26 groups (the supernatants of untreated CT26 cells were regarded as control group, CLSV group and CLSV/IL-23A group) were collected and incubated with cultured lymphocytes for 72 h. A mouse IFN-γ ELISA Kit (Thermo) was used to detect the level of IFN-γ secreted by lymphocytes in the supernatants following the manufacturer's guidelines. Subsequently, CT26 cells were pre-seeded in a 96-well plate (1×10^3 cells per well) and then exposed to the supernatants obtained from each group of lymphocytes for 48 h. The MTT assay was used to assess the viability and survival rate of CT26 cells.

Moreover, the supernatants collected from each group of lymphocytes was placed into CT26 cells were treated in six-well plates (1×10^3 cells/well) and cultured for 1 week. After fixation with 4% paraformaldehyde for 15 min, the cells were washed with PBS, stained with 0.1% crystal violet for 30 min, and wash away the excess crystal violet with PBS. The number of colonies was counted and photographed.

In vivo Tumor Inhibition Assay

All BALB/c female mice (6–8 weeks) experiments were conducted and approved under the guidance of the Animal Ethics Committee of the General Administration of Health Research of Sichuan University and The Guidelines and Standard Operating Procedure (SOP) for Laboratory Animals of Sichuan University. We next evaluated the therapeutic effect of CLSV/dual-mRNA complexes on different tumor models in 6–8-week-old BALB/c female mice. In the abdominal cavity metastatic model, these mice were intraperitoneally injected with CT26 cells (2×10^5 cells in 100 μL) on day 0. On day 2, the mice were randomly divided into five groups and administered daily intraperitoneal injections of normal saline (NS), CLSV (250 μg), CLSV/Bim (10 μg) complex, CLSV/IL-23A (10 μg), or CLSV/dual-mRNA complex (Bim/IL-23A, 10 μg/10 μg) for 14 treatments. On day 16, the mice were weighed and euthanized, and their tumors and internal organs (heart, liver, spleen, lungs, and kidneys) were harvested and preserved in 4% paraformaldehyde for further analysis.

In the subcutaneous tumor model, mice were subcutaneously injected with CT26 tumor cells (2.5×10^6 cells in 100 μL) on day 0. On day 3, the mice were randomly divided into five groups and received 14 treatments of NS, CLSV (250 μg), CLSV/Bim (10 μg) complex, CLSV/IL-23A (10 μg), or CLSV/dual-mRNA complex (Bim/IL-23A, 10 μg/10 μg) through intratumoral administration. Tumor volume changes were monitored every 2 days after injection. After 14 days of treatment, all mice were euthanized, and the tumors and internal organs were harvested and analyzed.

Immunohistochemistry Analysis

A series of immunological reactions of specific antibodies was employed to detect protein expression in the tumor tissue. The tumors were fixed with 4% paraformaldehyde to preserve their original morphological structure. Following fixation, the tissues underwent a series of steps, including dehydration, transparency, and embedding with paraffin wax. Slices of 3–4 μm thickness were carefully prepared from the paraffin-embedded tissue blocks. For histological analysis, hydrated sections were stained with hematoxylin and eosin (H&E) to visualize cellular structures. To detect apoptosis, a TUNEL kit from Promega (Madison, WI, USA) was used to stain the paraffin sections. For immunohistochemistry, after antigen retrieval, the sections were incubated overnight at 4°C with specific antibodies against Bim, CD31, caspase-9, caspase-3, CD4, IL-23A, and TNF-α (Abcam). Subsequently, the sections were incubated with HRP-conjugated secondary antibodies. Finally, the sections were observed and analyzed using a fluorescence microscope (Olympus, Japan).

Blood Tests

Eight female BALB/c mice were divided into two groups. The CLSV system group was intravenously injected with the CLSV system (250 μg) and the NS group was untreated. Blood was collected and analyzed after 24 h. The following indices were detected: white blood cell count (WBC), lymphocyte (Lymph), monocyte (Mon), neutrophil (Gran), platelet (LTT), red blood cell count (RBC), hemoglobin concentration (HGB), mean corpuscular hemoglobin concentration (MCHC), red blood cell specific volume (HCT), red blood cell distribution width (RDW), platelet distributing width (PCT), mean corpuscular volume (MCV), mean platelet volume (MPV), mean corpuscular hemoglobin (MCH), and platelet distribution width (PDW). The following serum parameters were measured: uric acid (UA), creatinine (CREA), aspartate aminotransferase (AST), urea nitrogen (UREA), and alanine aminotransferase (ALT).

Statistical Analysis

The data are presented as the mean ± standard deviation (SD). The data in the article were statistically analyzed by two-tailed *t*-test or one-way ANOVA using GraphPad Prism 8 software (GraphPad Software Inc., San Diego, CA, USA), and statistical significance was defined by a value of $P < 0.05$.

Results

Preparation and Characterization of the CLSV/mRNA Complex

In this study, a DMP nano-backbone was first formed through the self-assembly of the cationic lipid DOTAP and mPEG-PCL block polymer into nanosized micelles. To fuse with fCPP, the DMP nano-backbone was rendered active with maleimide-PEG-PCL (Mal-PEG-PCL), forming DMP-maleimide nanoparticles (DMP-mal). Then, CT26 tumor cell

lysate was packaged by DMP-mal forming DMP-mal-CT26 lysate. The fCPP was coupled with DMP-mal-CT26 lysate (Scheme 1) by maleimide-thiol Michael addition through chemical bonding to ensure the stability of the connection and the effective play of its function, thus obtaining an ideal mRNA delivery system (CLSV).

As measured by the nanosizer (Malvern ZS90, UK), the average diameter of the prepared DMP was 29.43 ± 3.09 nm (Figure 1A), with an average ζ-potential of +43 ± 0.7 mV (Figure 1B), and the average diameter of the prepared CLSV system was 241.17 ± 10 nm (Figure 1A), with an average ζ-potential of +39.53 ± 5.41 mV (Figure 1B). The morphology of the prepared DMP and CLSV system was further observed by TEM. As illustrated in Figure 1C and D, the CLSV nanoparticle exhibited regular spherical shape and the particle size was much larger than DMP, which indicated that CLSV nanoparticles were successfully synthesized. These measurements align with the results obtained from the nanosizer analysis. Besides, we used the BCA method to detect the initial concentration and the concentration after loading, and calculated the EE% values of CT26 cell lysate in CLSV system was 36.55 ± 2.39%, the LC% values of CT26 cell lysate in CLSV system was 2.90 ± 0.04%. And the conjugation rate of fCPP was calculated by HPLC method as 69.11%. In addition, we used FTIR and TGA methods to further characterize the successful formation of CLSV. Results of TGA were shown in Figure 1E, the degradation peak of the DMP and CLSV presented clear difference, thus suggesting CLSV was different with DMP and had been formed successfully. Besides, the similarities between CLSV before and after the purification step indicated that there were not many fCPPs unmodified. And the chemical structure of CLSV was analyzed by FTIR (Figure 1F). The strong peak at 1103 cm^{-1}correlated with C-S bone between DMP-mal and fCPP through maleimide-thiol Michael addition. The peak at 1725 cm^{-1} related to the stretching vibration of carbonyl groups in mPEG-PCL. There results indicated that CLSV nanoparticles were successful formulation and could be used in subsequent experiments.

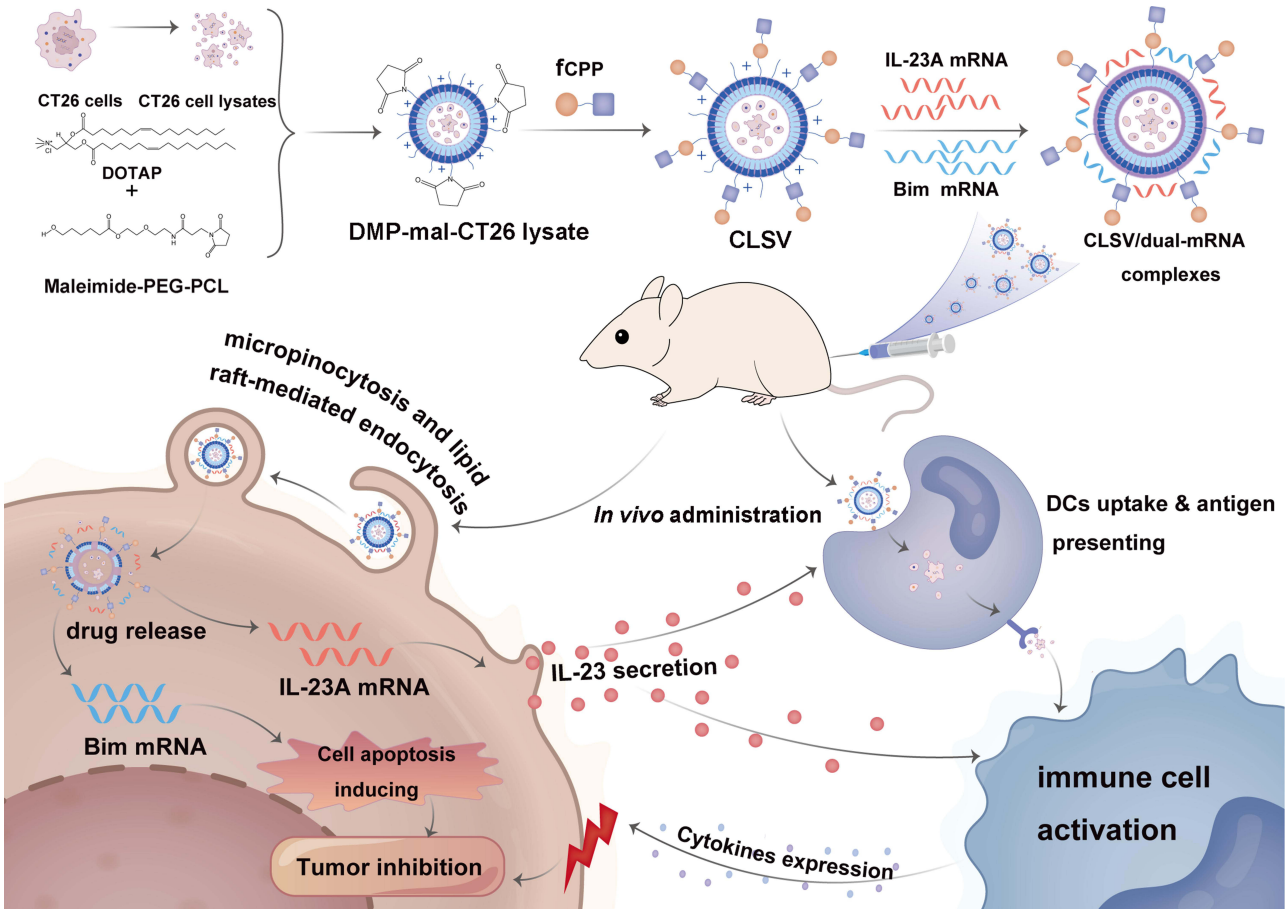

Scheme 1 A schematic view of the formulation and therapeutic processes of the CLSV/dual-mRNA complex.

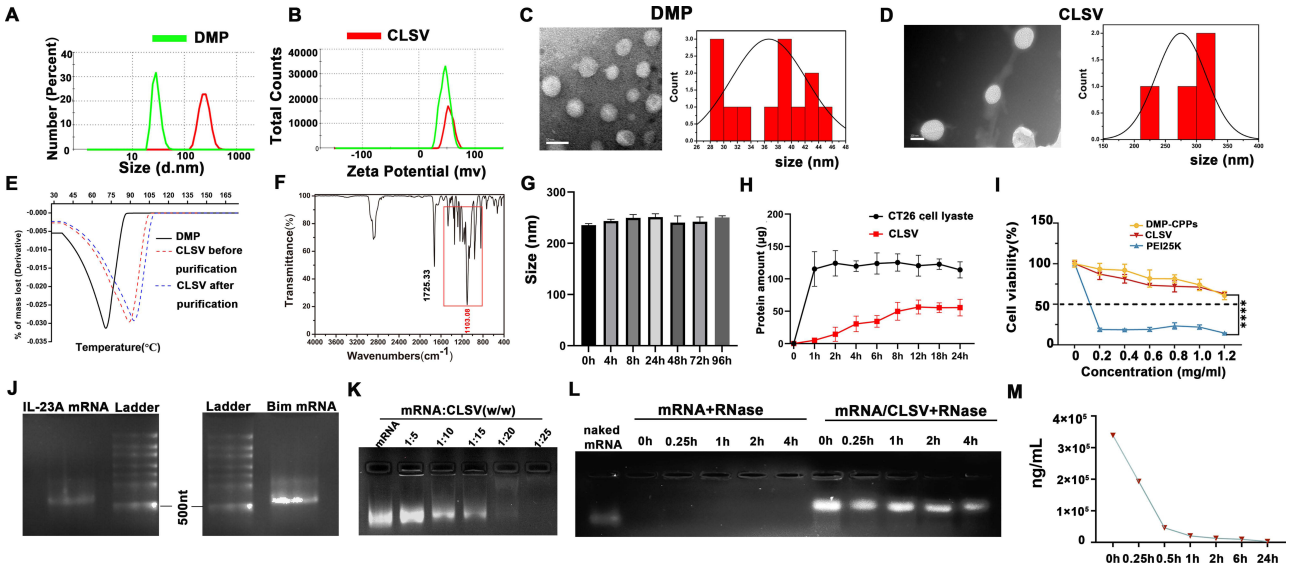

Figure 1 Characterization of the CLSV system. (**A**) Size distribution of the DOTAP-mPEG-PCL (DMP) and CLSV systems. (**B**) Zeta potential of the DMP and CLSV systems. (**C**) TEM photomicrographs and the TEM histogram of the DMP (scale bar: 50 nm). (**D**) TEM photomicrographs and the TEM histogram of CLSV systems (scale bar: 200 nm). (**E**) Thermogravimetric analysis of CLSV before and after purification with control DMP. (**F**) Fourier-transform infrared spectroscopy (FTIR) spectra of CLSV (**G**) The size of CLSV nanoparticles in different time in normal saline. (**H**) The protein amounts of CT26 cell lysates released by CLSV nanoparticles in phosphate-buffered saline (PBS) at different time points. (**I**) Cell viability assay of PEI25K, DMP-CPPs, and CLSV on 293T cells (n = 3; ****P < 0.0001). (**J**) Gel electrophoresis to verify the murine IL-23A-encoded mRNA bands and Bim-encoded mRNA bands. (**K**) Gel retarding assay of the CLSV/mRNA complex. (**L**) RNase protection assay of the CLSV/mRNA complex. (**M**) the content of CLSV nanoparticles in different time (0 h, 0.25 h, 0.5 h, 1 h, 2 h, 6 h, 24 h) in mice blood.

Besides, to evaluate in vitro the stability of prepared CLSV nanoparticles in normal saline to mimic in vivo condition, we measured the size of CLSV nanoparticles in different time (0 h, 4 h, 8 h, 24 h, 48 h,72 h,96 h), the result was as shown in Figure 1G, suggesting that CLSV nanoparticles were still keep stability in vivo condition. Moreover, to investigate whether CLSV can release CT26 cell lysates in vitro, we placed the same batch of prepared cell lysates and CLSV with equal protein quality in the pore plate respectively, and incubated them in the cell incubator after adding PBS to simulate the in vivo environment. By testing the protein quality in the pore at different time points, the results as shown in the Figure 1H indicated that CLSV could slowly release cell lysates in PBS.

The MTT assay was used to measure CLSV cytotoxicity against CT26 cells. As illustrated in Figure 1I, the IC50 values for both the DMP-CPPs and CLSV system exceeded 1200 μg/mL, whereas PEI25K had an IC50 value < 100 μg/mL ($P < 0.0001$). This implied that the CLSV system exhibited a higher level of safety than PEI25K. We synthesized Bim mRNA and IL-23A mRNA using a T7 polymerase-based IVT method, followed by 5′-end capping and 3′-end tail modification. Agarose gel electrophoresis was then performed to confirm the successful synthesis of IVT mRNA. As shown in Figure 1J, bands of Bim and IL-23A mRNAs were as expected, with bands of approximately 591 nucleotides illuminated on the gel. The CLSV system was then mixed with negatively charged mRNA to form the CLSV/dual-mRNA complex (Scheme 1). As shown in Figure 1B, the CLSV system ζ-potential was +39.53 mV, indicating that the CLSV system and mRNA were complexed through electrostatic binding and retained the nanosized structure. We then investigated the ability of the CLSV system to bind to mRNA. According to our results, when the mass ratio of the CLSV system to mRNA was 25:1, the mRNA bands in the agarose gel were almost invisible, indicating that the CLSV system could completely bind mRNA at this ratio (Figure 1K). We further characterized the ability of the CLSV system to protect against mRNA. As shown in Figure 1L, free mRNA was completely degraded by RNase within 15 min, whereas the CLSV system effectively protected mRNA against RNase degradation for up to 4 h. No obvious decrease in the brightness of the mRNA band was observed between each time point. These results suggested that the synthetic CLSV nanoparticles effectively bound and protected mRNA. And then we detect the content of CLSV nanoparticles in different time in mice blood, the pharmacokinetics results (Figure 1M) showed that CLSV nanoparticles had longer circulation profile, with a half-life of >1h. Additionally, the presence of CLSV nanoparticles could still be detected even at 24 hours

post-administration. This suggested that CLSV nanoparticles possessed the capability to prolong the presence of the drug in the systemic circulation, potentially enhancing its therapeutic effects.

In vitro Transfection Study

We then evaluated the efficiency with which the CLSV system delivered mRNA in vitro. According to our results, the CLSV system delivered EGFP-encoded mRNA and mCherry-encoded mRNA into CT26 and 293T cells with high efficiency (Figure 2A). The transfection efficiency of EGFP mRNA and mCherry mRNA simultaneously delivered by CLSV into CT26 cells reached 71.58% and 62.18%, respectively, which was similar to that of transfection with DMP-CPPs (EGFP mRNA: 70.91%; mCherry mRNA: 59.88%) (Figure 2B). In addition, the transfection of CLSV was much higher than that of unmodified DMP (EGFP mRNA: 54.26%, $P < 0.0001$; mCherry mRNA: 48.58%, $P < 0.0001$) and the gold standard transfection agent, PEI 25K (EGFP mRNA: 28.82%, $P < 0.0001$; mCherry mRNA: 17.68%, $P < 0.0001$) (Figure 2B). This strong mRNA delivery ability of the CLSV system was also verified with 293T cells. In this case, the transfection efficiency of EGFP mRNA and mCherry mRNA in the CLSV system reached 87.67% and 78.16%, respectively, which was similar to that of DMP-CPPs (EGFP mRNA: 84.4%; mCherry mRNA: 73.24%), and those values was higher than the values for DMP (EGFP mRNA: 76.11%, $P < 0.0001$; mCherry mRNA: 64.75%, $P < 0.001$) and PEI25K (EGFP mRNA: 48.92%, $P < 0.0001$; mCherry mRNA: 47.24%, $P < 0.0001$) (Figure 2C). These results demonstrated that the CLSV system could safely and efficiently deliver two mRNAs into cells simultaneously in vitro.

The mechanism used by cells to take up the CLSV/mRNA complex was further studied. Generally, four endocytosis internalization mechanisms are used for the cellular uptake of nanosized cargos. Before transfection, we exposed CT26 cells to different well-known inhibitors, including wortmannin for micropinocytosis, filipin III and genistein for caveolin-mediated endocytosis, chlorpromazine for clathrin-mediated endocytosis, and methyl-β-cyclodextrin for lipid raft-mediated endocytosis.[27,28]

Forty-eight hours after transfection, we observed an obvious reduction in both efficiency and fluorescence intensity in the wortmannin-treated group compared with the untreated group, as illustrated in Figure 2D. Compared with the untreated group, a noticeable decrease in transfection efficiency, amounting to nearly 30% ($P < 0.0001$), was evident in cells that had been pretreated with wortmannin, as shown in Figure 2E. Additionally, methyl-β-cyclodextrin-mediated lipid raft endocytosis led to a decrease in transfection efficiency, amounting to nearly 15% ($P < 0.001$). These results suggested that micropinocytosis and lipid raft endocytosis played a more prominent role than the other pathways in facilitating the transmembrane transportation of the CLSV/mRNA complex by CT26 cells, ultimately leading to high delivery efficiency.

In addition, as shown in Figure 2F and 2G, there was no significant change in the transfection efficiency of CLSV nanoparticles at different serum concentrations (0%, 2%, 4%, 6%, 8%, 10%), indicating that CLSV nanoparticles could still keep stability to deliver mRNA into cells when serum was present in vivo conditions.

CLSV System Efficiently Activated the Systemic Immune Response Both in vitro and in vivo

We next investigated the immune stimulation ability of the CLSV system. As DCs play a primary role in antigen processing, we first examined the uptake ability of BMDCs, as shown in Figure 3A. After incubation with the Cy5.5-labeled CLSV system for 24 h, the CLSV system showed obvious uptake into the cytoplasm by BMDCs. We then investigated the effects of the CLSV system on DC maturation through flow cytometry (Figure 3B and C). According to our results (Figure 3D), the percentage of mature BMDCs ($CD11C^+$ $CD80^+$ $CD86^+$) in the CLSV group was 71.24% ± 3.96%, which was much higher than those in the NS (38.03% ± 1.25%, $P < 0.001$), DMP-CPPs (51.33% ± 6.86%, $P < 0.01$), and tumor cell lysate (51.61% ± 5.78%, $P < 0.01$) groups. Moreover, compared with the CLSV group, the percentage of mature BMDCs ($CD11C^+$ $CD80^+$ $CD86^+$) was decreased by nearly 19.91% in the DMP-CPPs group and by nearly 19.63% in the tumor cell lysate group, among which CLSV demonstrated the strongest ability to induce BMDC maturation. The expression of MHC on the DC surface plays a key role in antigen presentation and recognition of T cells. We then investigated the effects of DMP-CPPs, tumor cell lysate, and the CLSV system on DC antigen

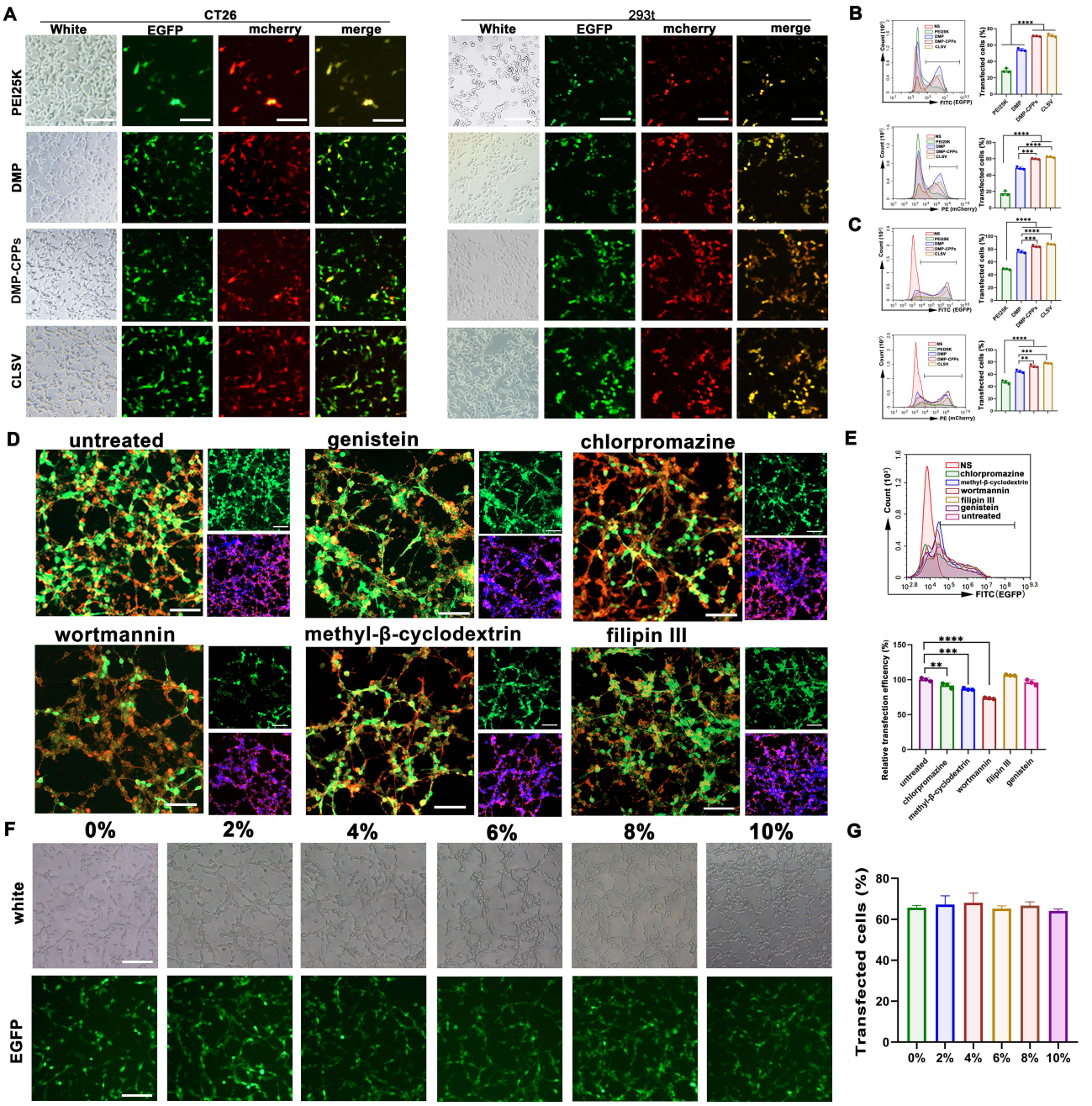

Figure 2 In vitro gene transfection by the CLSV/mRNA complex. (**A**) Fluorescence microscopy images of CT26 and 293T cells (scale bar: 100 μm). (**B**) EGFP mRNA efficiency of CT26 cell transfection (n = 3; ****P < 0.0001) and mCherry mRNA efficiency (n = 3; ***P < 0.001 and ****P < 0.0001) analyzed by flow cytometry. (**C**) EGFP mRNA efficiency of 293T cell transfection (n = 3; ***P < 0.001 and ****P < 0.0001) and mCherry mRNA efficiency (n = 3; **P < 0.01, ***P < 0.001, and ****P < 0.0001) analyzed by flow cytometry. (**D**) Fluorescent images of internalization of the CLSV/mRNA complex after treatment with various inhibitors (scale bar: 100 μm). (**E**) The uptake rates were analyzed by flow cytometry (n = 3; **P < 0.01, ***P < 0.001, and ****P < 0.0001). (**F**) Transfection ability of CLSV nanoparticles in serum with different concentrations (scale bar: 100 μm). (**G**) EGFP mRNA transfection efficiency of CT26 cell in serum with different concentrations analyzed by flow cytometry.

presentation. Similarly, according to our results (Figure 3E), the percentage of MHC-II$^+$ (CD11C$^+$ MHC-II$^+$) BMDCs in the CLSV group was 76.56% ± 6.51%, which was also greater than those in the DMP-CPPs (56.26% ± 2.62%, P < 0.001), tumor cell lysate (62.47% ± 1.91%, P < 0.5), and NS (43.98% ± 1.73%, P < 0.0001) groups. Moreover, compared with the CLSV group, the percentage of mature MHC-II$^+$ (CD11C$^+$ MHC-II$^+$) BMDCs decreased by nearly 20.3% in the DMP-CPPs group and nearly 14.09% in the tumor cell lysate group, among which CLSV demonstrated the most potent ability to induce MHC-II expression. These results indicated that the activation and maturation of DCs could be induced

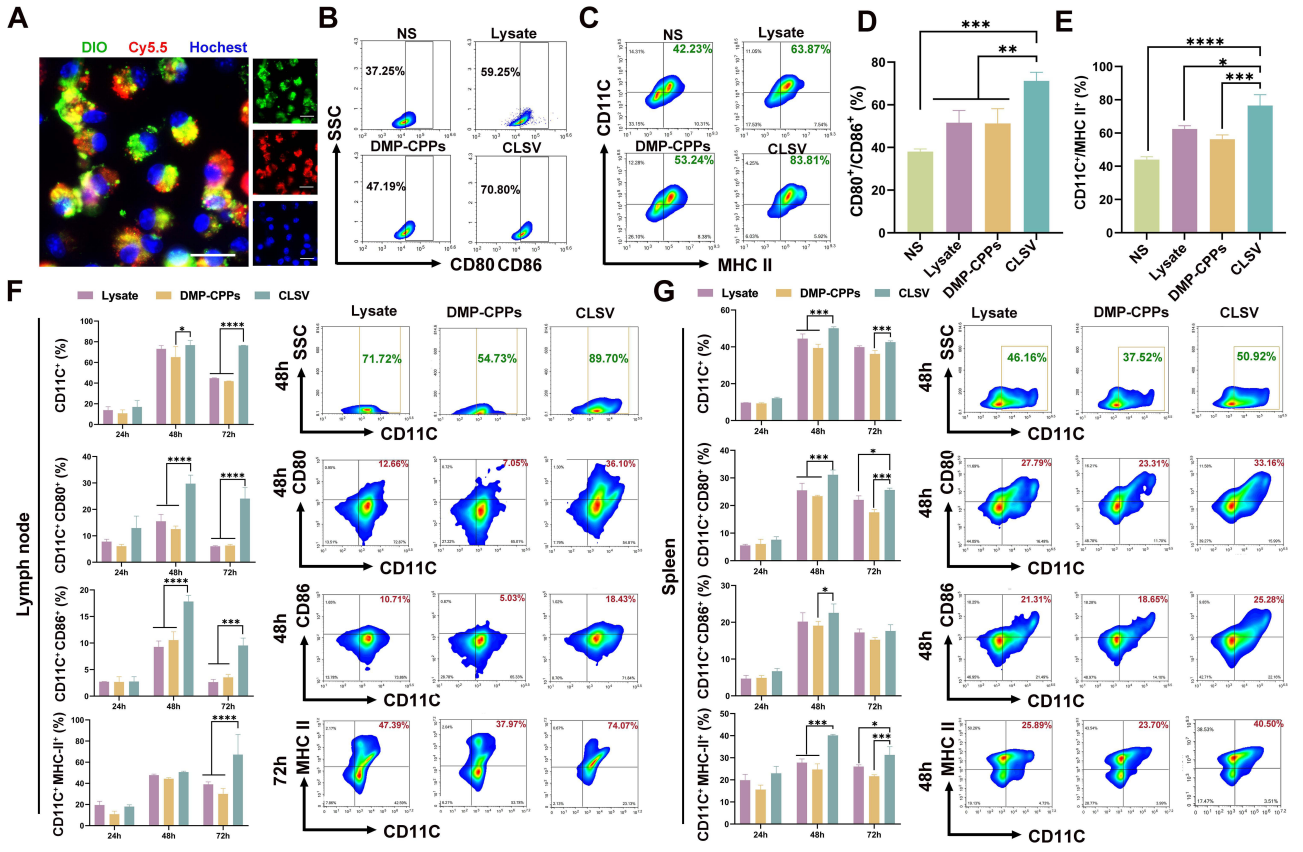

Figure 3 CLSV system activates immunity in vitro and in vivo. (**A**) Colocalization study of BMDC uptake of CLSV (scale bar: 20 μm). (**B** and **C**) Expression of CD11C$^+$ CD80$^+$ CD86$^+$ (**B**) and CD11C$^+$ MHC II$^+$ in BMDCs in vitro (**C**). (**D** and **E**) Ratio of the expression of CD11C$^+$ CD80$^+$ CD86$^+$ (**D**) and CD11C$^+$ MHC II$^+$ by flow cytometry in BMDCs in vitro (**E**) (n = 3; *P < 0.05, **P < 0.01, ***P < 0.001, and ****P < 0.0001). (**F** and **G**) Expression of CD11C$^+$, CD80$^+$, CD86$^+$, and MHC-II$^+$ mouse lymph node lymphocytes (**F**) and mouse splenic lymphocytes (**G**) after treatment with DMP-CPPs, tumor cell lysate, and CLSV (n = 3; *P < 0.05, ***P < 0.001, and ****P < 0.0001).

by empty DMP-CPPs nanoparticles, which is rare in non-viral vectors. Moreover, although DCs could be activated by tumor cell lysate alone, the immune stimulation capacity was further elevated after encapsulation of CT26 tumor cell lysate into the DMP skeleton. Compared with the DMP-CPPs and lysate, the stimulation effect of CLSV appeared to be a superposition of them, implying an adjuvant-like property of DMP-CPPs. Our results also suggested that the CLSV system could more effectively induce the maturation and activation of BMDCs in vitro.

To further verify the systemic immunostimulatory effect of the CLSV system in vivo, mice were injected with DMP-CPPs, tumor cell lysate, or the CLSV system, and the related parameters in in lymph nodes (LNs) and spleens were monitored for 72 h. As shown in Figure 3F, administration of the CLSV system increased the number of CD11C$^+$ cells (89.7%, peak value at 48 h), mature DCs (CD11C$^+$ CD80$^+$ (36.10%) and CD11C$^+$CD86$^+$ (18.43%, peak value at 48 h), and MHC-II$^+$ DCs (74.07%, peak value at 72 h) in the LNs, with similar effects detected in the spleen. Administration of the CLSV system increased the number of CD11C$^+$ cells (50.92%, peak value at 48 h), mature DCs (CD11C$^+$ CD80$^+$ (33.16%) and CD11C$^+$CD86$^+$ (25.28%), peak value at 48 h), and MHC-II$^+$ DCs (40.50%, peak value at 48 h) in the spleen (Figure 3G). Consistent with the in vitro results, empty DMP-CPPs nanoparticles also demonstrated immune ability in vivo. Our results further showed that the restricted immune stimulation capacity of lysate injection alone and the resulting effect were elevated after encapsulation into DMP-CPPs nanoparticles. These results indicated that the DMP-CPPs skeleton could act as an adjuvant during the immune activation process. Therefore, these results indicated that the CLSV system could efficiently induce the activation and maturation of DCs, suggesting strong immune therapeutic potential in vivo.

CLSV/Bim Complex Inhibits CT26 Cell Proliferation in vitro

We subsequently explored the mechanism through which the CLSV/Bim complex inhibits the proliferation of cancer cells in vitro. Initially, we assessed whether treatment with the CLSV/Bim complex led to elevated levels of Bim mRNA

and protein. Our qRT–PCR analysis revealed a substantial increase in Bim mRNA levels in the CLSV/Bim complex-treated group, showing a 3.8 × 10^4-fold rise compared with cells treated with CLSV alone ($P < 0.0001$) (Figure 4A). Furthermore, the expression of the Bim protein exhibited a significant increase in the CLSV/Bim complex-treated group compared to the NS and CLSV groups (Figure 4B). These results affirmed that CLSV effectively delivered Bim mRNA into CT26 cells with remarkable efficiency.

Subsequently, we examined the anti-proliferative effects of the CLSV/Bim complex using an MTT assay. Our results showed that CT26 cell viability was significantly reduced after treatment with the CLSV/Bim complex (Figure 4C). Compared with the untreated group, only 11.75% of cells survived in the Bim/CLSV complex-treated group, indicating significantly lower cell viability than that in the CLSV-treated group (62.57%; $P < 0.0001$) (Figure 4D). We further assessed the ability of the Bim/CLSV complex to inhibit cell growth using clonogenic assays. As illustrated in Figure 4E and F, the CLSV/Bim complex treatment group exhibited a reduced number of CT26 cell colonies, with an average count of 11 ± 6 colonies and an average inhibition rate of 93.67% ($P < 0.0001$), compare to the untreated group (Figure 4E and F). In contrast, the untreated and CLSV-treated groups displayed significantly more colonies, with counts of 173 ± 14 ($P < 0.0001$) and 126 ± 2 ($P < 0.0001$), respectively (Figure 4E and F). These findings underscore the high efficiency of the CLSV/Bim complex in delivering Bim mRNA to CT26 cells and its robust ability to inhibit CT26 cell growth in vitro.

As a significant protein within the Bcl-2 family, Bim triggers apoptosis. Therefore, we examined whether the suppressive effect of the CLSV/Bim complex was linked to the induction of apoptosis. Our results revealed that

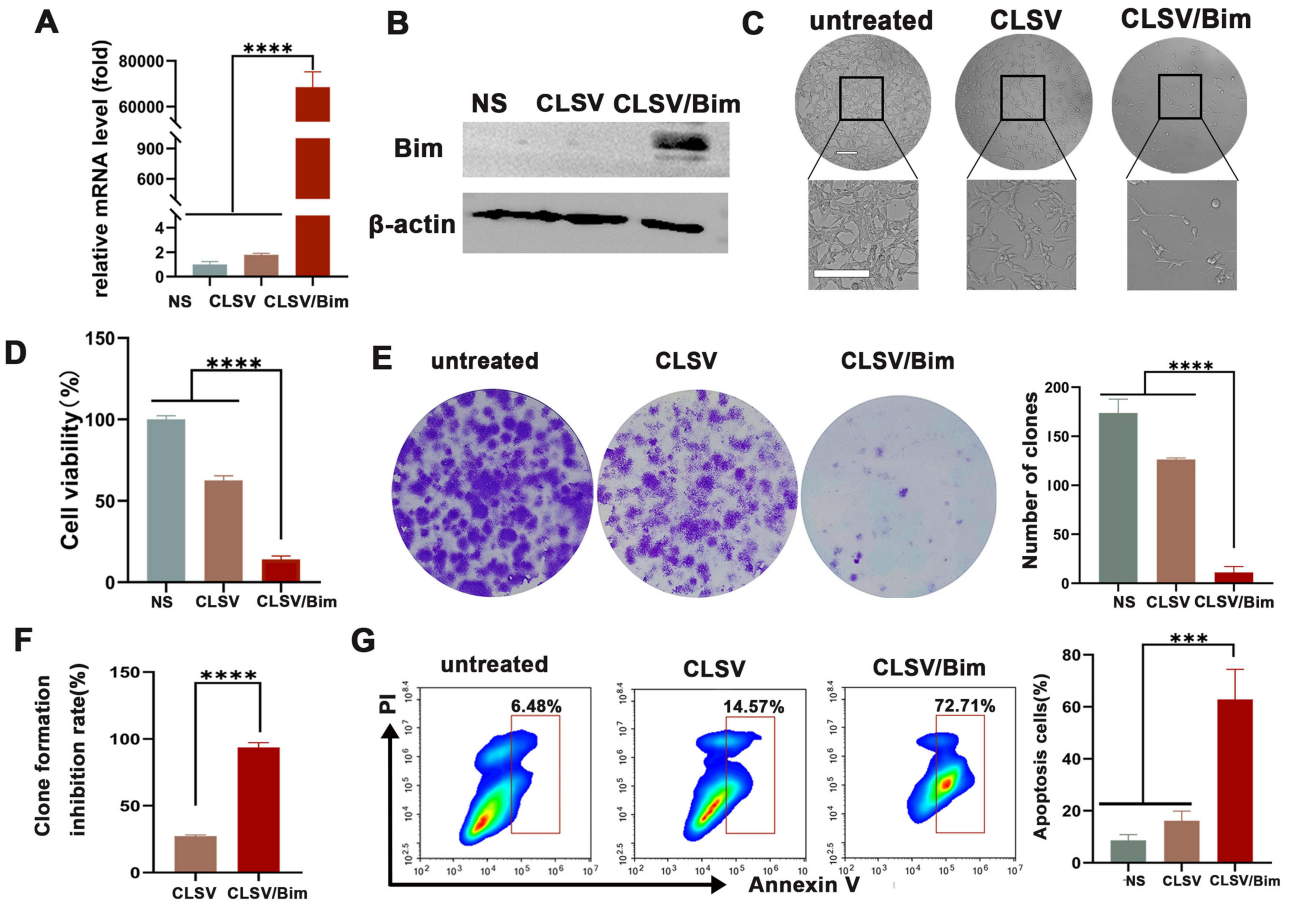

Figure 4 CLSV/Bim complex inhibited CT26 cell proliferation in vitro. (**A**) Bim mRNA levels in CT26 cells after transfection (n = 3; ****P < 0.0001). (**B**) The level of the Bim protein. (**C** and **D**) CT26 cells after treatment with the CLSV/Bim complex (scale bar: 100 μm) and the cell viability in each group was measured using the MTT assay (n = 3; ****P < 0.0001). (**E** and **F**) Detection of the anti-proliferative effect of the CLSV/Bim complex using the clonogenic assay and inhibition rates were calculated on the basis of clone numbers (n = 3; ****P < 0.0001). (**G**) The CLSV/Bim complex efficiently induced apoptosis in CT26 cells as determined by flow cytometry (n = 3; ***P < 0.001).

compared with the CLSV groups, the CLSV/Bim complex clearly induced apoptosis (Figure 4G). By using Annexin V/PI staining, we determined that the apoptotic cell rate in the CLSV/Bim complex-treated group was 62.85% compared with only 16.15% for the CLSV groups ($P < 0.001$) (Figure 4G). These findings suggested that the CLSV/Bim complex effectively inhibited CT26 cell growth by inducing mitochondria-dependent apoptosis.

CLSV/IL-23A mRNA Complex Efficiently Inhibited Colon Cancer Cells in vitro

We then assessed the in vitro anti-tumor potential of the CLSV/IL-23A complex (Figure 5A). Initially, we assessed the intracellular IL-23A mRNA levels in CT26 cells. As depicted in Figure 5B, compared with the untreated group, the CLSV/IL-23A group exhibited a remarkable 34,813-fold increase in IL-23A mRNA levels ($P < 0.0001$). We also investigated IL-23A protein expression using ELISA. According to our results, the CLSV/IL-23A group displayed an IL-23A protein level of 85.28 pg/mL after 96 h of treatment (Figure 5C). These findings strongly indicate the successful delivery of IL-23A mRNA into CT26 cells by CLSV with high efficiency.

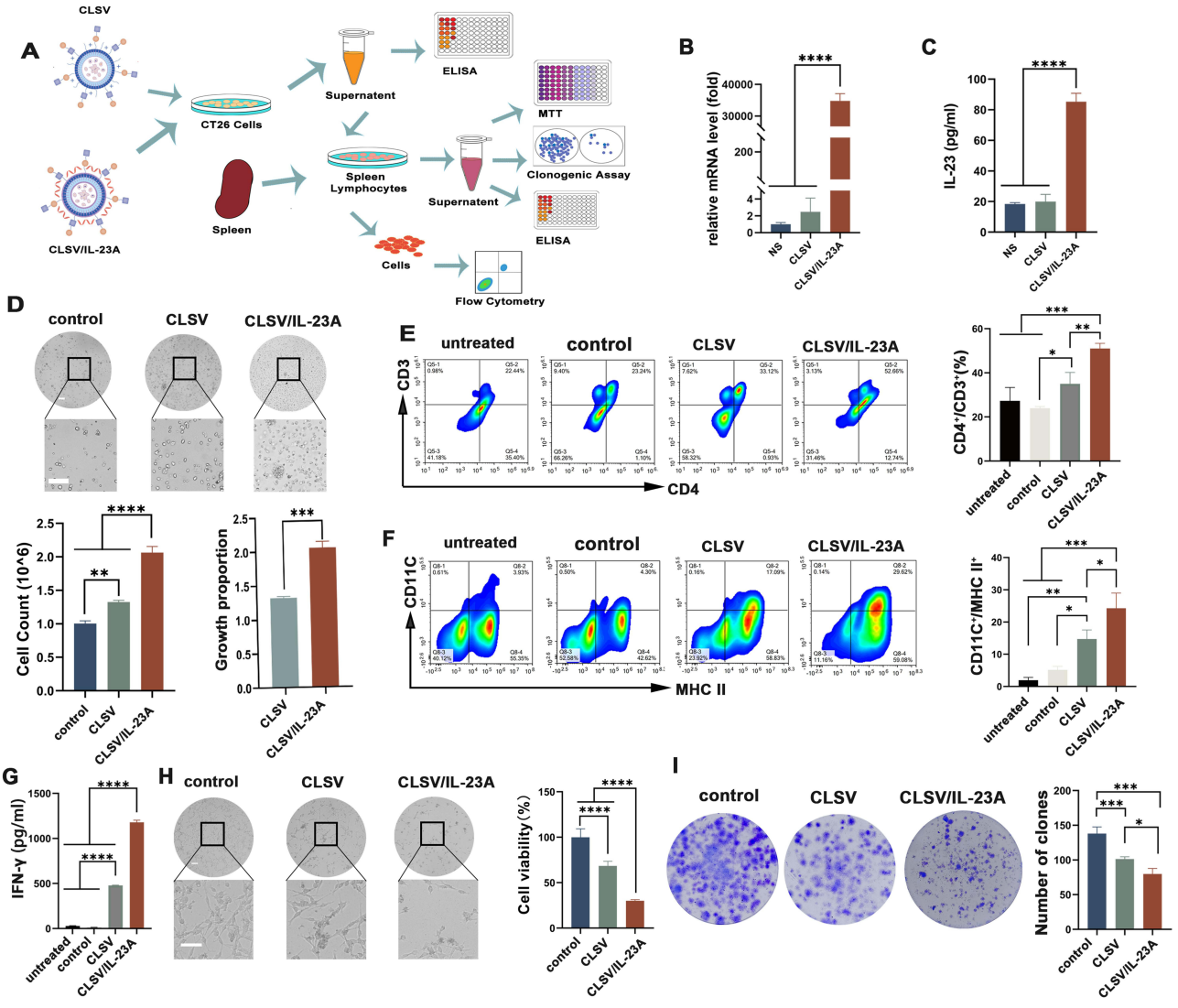

Figure 5 Anti-tumor effects of the CLSV/IL-23A complex by lymphocyte-based stimulation in vitro. (**A**) Experimental design of the splenic lymphocyte supernatant anti-tumor assay. (**B**) Level of IL-23A mRNA in CT26 cells after transfection (n = 3; ****P < 0.0001). (**C**) Concentration of IL-23A in the supernatant after CLSV/IL-23A complex transfection of CT26 cells (n = 3; ****P < 0.0001). (**D**) Microscopic images of lymphocyte proliferation after stimulation with the supernatant of CT26 cells (scale bar: 100 μm; n = 3, **P < 0.01, ***P < 0.001, and ****P < 0.0001). (**E** and **F**) Activation of DCs and T cells detected by flow cytometry (n = 3; *P < 0.05, **P < 0.01, and ***P < 0.001). (**G**) IFN-γ level in the supernatant of lymphocytes as detected by ELISA (n = 3; ****P < 0.0001). (**H**) CT26 cells were treated with lymphocyte supernatant for viability assay (n = 3; scale bar: 100 μm; ****P < 0.0001) (**I**) A clonogenic assay was used to detect the anti-tumor effect of lymphocyte-mediated cytotoxicity (n = 3; *P < 0.05 and ***P < 0.001).

https://doi.org/10.2147/IJN.S452548 DovePress

Subsequently, we explored whether the expressed IL-23A could promote lymphocyte proliferation. To this end, we treated mouse spleen-derived lymphocytes with supernatant from CT26 cells pretreated with the CLSV/IL-23A complex. Our results revealed observable stimulatory effects on proliferation under a microscope (Figure 5D). Analysis of cell counts revealed a significant increase in the lymphocyte cell count in the CLSV/IL-23A-treated group (2.06×10^6) compared with that in the control group (1.00×10^6) ($P < 0.0001$) and in the CLSV group (1.33×10^6) ($P < 0.0001$).

We further investigated specific activation effects among lymphocytes. As shown in Figure 5E and F, compared with the other groups, treatment with CLSV/IL-23A notably increased the numbers of $CD3^+$ $CD4^+$ cells (51.04% ± 2.34%; untreated, 23.31% ± 6.08%, $P < 0.001$; control, 23.99% ± 0.72%, $P < 0.001$; and CLSV, 35.01% ± 5.14%, $P < 0.01$) and $CD11C^+$ MHC II^+ cells (24.27% ± 4.71%; untreated, 3.49% ± 1.02%, $P < 0.001$; control, 5.16% ± 1.08%, $P < 0.001$; and CLSV, 14.75% ± 2.79%, $P < 0.5$). These findings suggest that IL-23A delivered by CLSV effectively facilitates the in vitro proliferation and activation of various lymphocytes, including DCs and T cells.

To further investigate the impact of lymphocyte activation on CT26 cells, we exposed CT26 cells to the supernatant obtained from lymphocytes treated as described earlier. We used ELISA to detect the concentration of IFN-γ in the supernatant obtained from lymphocytes, which, in the CLSV/IL-23A complex group, reached 1178.9 pg/mL (Figure 5G). Our results also revealed distinct morphological changes in the CLSV/IL-23A treatment group, including cell crumpling and aggregation. Subsequently, the cell viabilities were assessed using the MTT assay. As depicted in Figure 5H, treatment with the CLSV/IL-23A complex led to notable inhibition of CT26 cell proliferation. Compared with the untreated group, the survival rate in the CLSV/IL-23A group decreased by 70.47% ($P < 0.0001$), which was notably higher than that in the CLSV group (31.74%, $P < 0.0001$). We further evaluated the anti-proliferative potential of the CLSV/IL-23A complex using a clonogenic assay. As illustrated in Figure 5I, significantly fewer cell clones were observed in the CLSV/IL-23A treatment group (74 ± 15) than in the other groups (148 ± 5 for the CLSV group, $P < 0.05$; 151 ± 14 for the control group, $P < 0.001$). These results collectively demonstrated that CLSV could effectively deliver IL-23A mRNA into CT26 tumor cells, leading to enhanced secretion of IL-23A protein, while the CLSV/IL-23A complex suppressed the proliferation of CT26 cells by activating lymphocytes.

Local Administration of the CLSV/Dual-mRNA Complex Efficiently Suppressed Tumor Growth

We then verified the treatment effect of the CLSV/dual-mRNA complex through local administration. The therapeutic efficacy of the CLSV/dual-mRNA complex was first validated in an abdominal cavity metastatic model using intraperitoneal injection (Figure 6A). As depicted in Figure 6B, the CLSV/dual-mRNA complex group had fewer metastatic tumor nodules (white arrows) compared to other groups, suggesting a significant anti-tumor effect. We then harvested the abdominal tumor nodules, and the results demonstrated that the average number of nodules in the CLSV/dual-mRNA complex group was significantly lower than that in the other groups (Figure 6C). The number of tumor nodes for the CLSV/dual-mRNA complex group was 7 ± 3, while those for the CLSV/Bim, CLSV/IL-23A, CLSV, and NS groups were 24 ± 6 ($P < 0.01$), 47± 21 ($P < 0.01$), 61 ± 12 ($P < 0.001$), and 134 ± 60 ($P < 0.01$), respectively (Figure 6D). Similarly, a lower average tumor weight (0.10 ± 0.08 g) was calculated in the CLSV/dual-mRNA group than in the CLSV/Bim (0.66 ± 0.22 g, $P < 0.01$), CLSV/IL-23A (0.69 ± 0.39 g, $P < 0.01$), CLSV (1.33 ± 0.18 g, $P < 0.001$), and NS (2.40 ± 0.53 g, $P < 0.01$) groups (Figure 6E), which resulted in a 95.8% inhibition rate in the CLSV/dual-mRNA complex group ($P < 0.0001$) (Figure 6F). These results suggest that intraperitoneal injection of the CLSV/dual-mRNA complex was more effective in inhibiting the growth of intraperitoneal metastases, although intraperitoneal injection of the single mRNA group had anti-cancer effects.

We then employed immunohistochemistry and immunofluorescence to verify the therapeutic mechanism of the CLSV/dual-mRNA complex (Figure 6G). The results showed that Bim and IL-23A protein expression in the CLSV/dual-mRNA complex group was similar to that in the CLSV/Bim and CLSV/IL-23A groups, which was higher than that in the NS and CLSV groups. This strongly suggest the effective delivery of Bim and IL-23A mRNAs into tumor tissues through the CLSV system (Figure 6G). The TUNEL results indicated an obvious increase in apoptosis levels following treatment with the CLSV/dual-mRNA complex, even though the CLSV/Bim and CLSV/IL-23A groups also showed apoptosis effects on tumor cells (Figure 6G). Moreover, CD31 staining revealed that microvessel density was

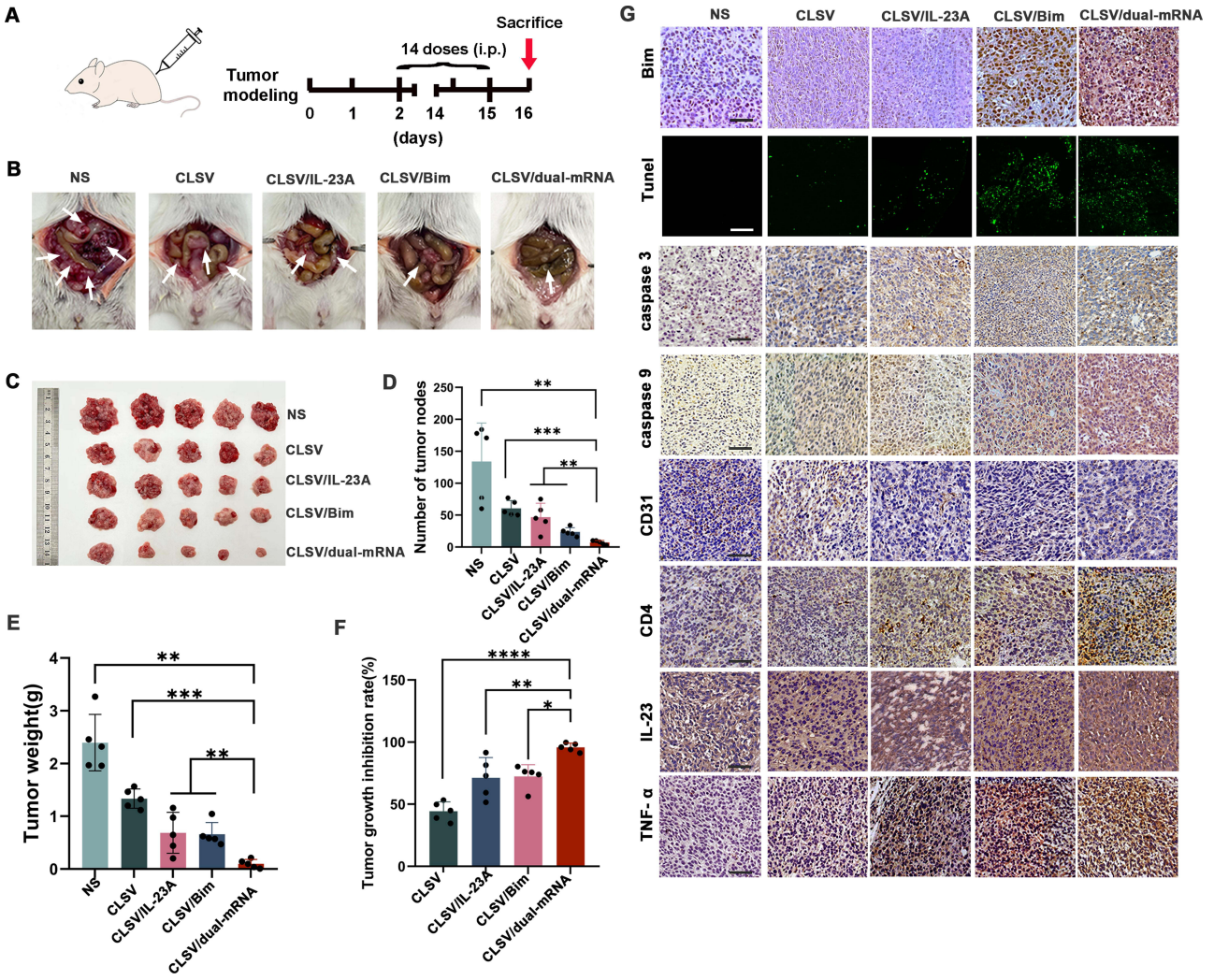

Figure 6 CLSV/dual-mRNA complex inhibited abdominal cavity metastatic tumor growth in vivo. (**A**) Schematic representation of the experimental design. (**B**) Images of representative mice from each treatment group. (**C**) Tumor nodules harvested from each group. (**D**) The average number of tumor nodules in each group (**P < 0.01 and ***P < 0.001). (**E**) The average tumor weight in each group (**P < 0.01 and ***P < 0.001). (**F**) The tumor growth inhibition rate in each group (*P < 0.05, **P < 0.01, and ****P < 0.0001). (**G**) Immunohistochemical evaluation of tumor tissues (scale bars: 50 μm).

significantly decreased in the CLSV/dual-mRNA complex group compared with other groups, indicating an anti-angiogenesis effect of the CLSV/dual-mRNA complex. In addition, strong positive signals from caspase-9 and caspase-3 proteins were observed in tumor sections from the CLSV/dual-mRNA complex group, suggesting obvious apoptosis induction (Figure 6G).

The CLSV/dual-mRNA complex was also found to enhance immune cell infiltration. Our results showed that the levels of the CD4 and TNF-α markers were increased after treatment with the CLSV/dual-mRNA complex, demonstrating the CLSV/dual-mRNA complex has the ability to activate and recruit immune cells in the CLSV/dual-mRNA complex (Figure 6G). These results further indicate the activation of immune responses during CLSV/dual-mRNA complex treatment. These results imply that the CLSV/dual-mRNA complex, through immune stimulation, apoptosis induction, and antiangiogenic effects, effectively inhibits the growth of CT26 tumor metastases.

Similarly, we also verified the anti-tumor effect of the CLSV/dual-mRNA complex on CT26 subcutaneous xenografted colon cancer through intratumoral injection (Figure 7A). The tumor growth curve and photograph of harvested tumors showed that the CLSV/dual-mRNA complex exerted an anti-tumor effect (Figure 7B and C). As depicted in Figure 7B and C, the tumors of the CLSV/dual-mRNA groups grew slowly. At the treatment endpoint, the average tumor volume for the CLSV/dual-mRNA complex group was 210 ± 66 mm^3, which was much smaller than those of the CLSV/Bim (338 ± 108 mm^3; P < 0.05), the CLSV/

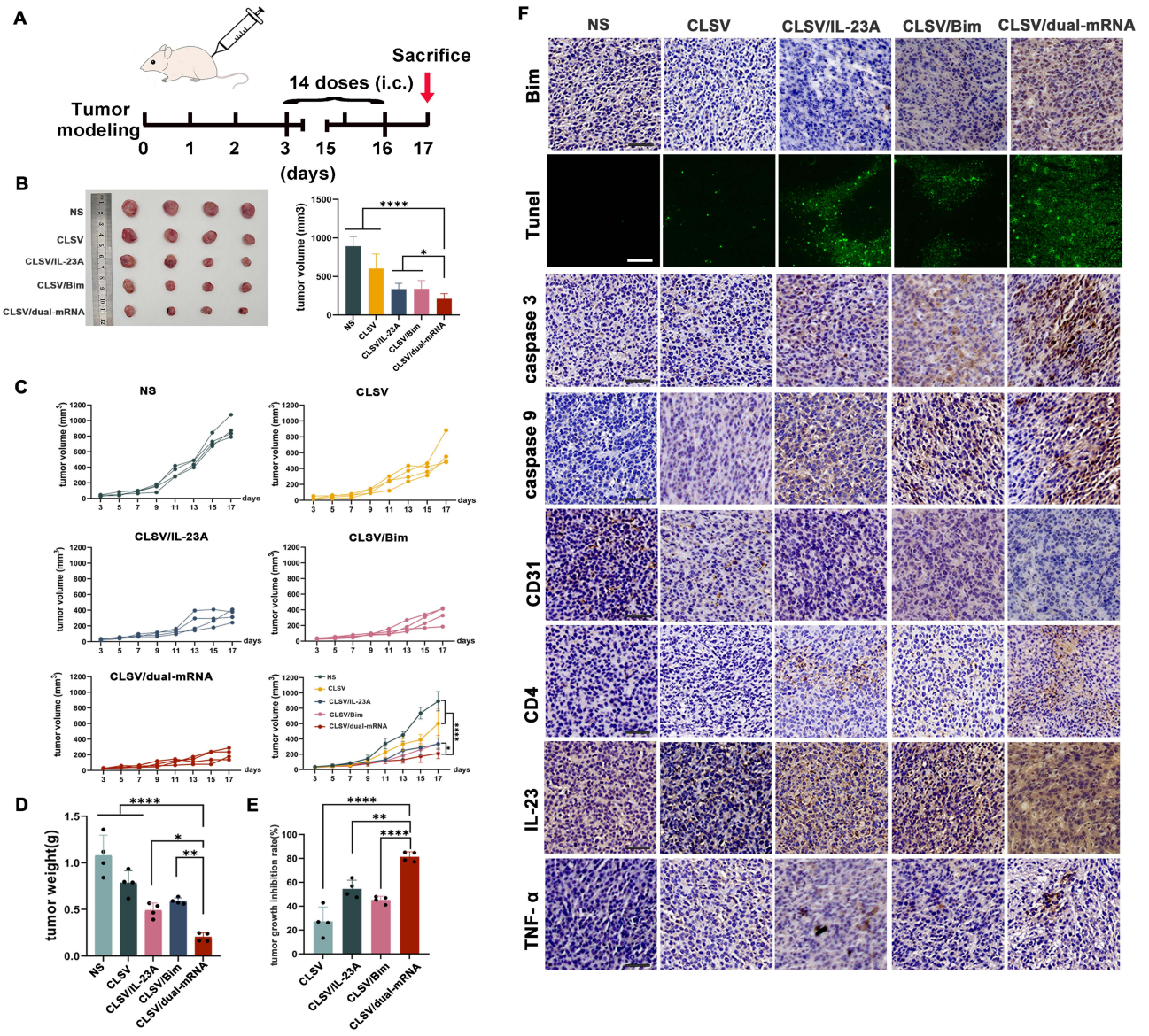

Figure 7 CLSV/dual-mRNA complex suppressing the CT26 subcutaneous xenograft model in vivo. (**A**) Schematic representation of the experimental design. (**B**) Images of tumors collected from each group. (**C**) Tumor growth curves from each treatment group (*P < 0.05 and ****P < 0.0001). (**D**) Average tumor weights (*P < 0.05, **P < 0.01, and ****P < 0.0001). (**E**) The tumor growth inhibition rate in each group (**P < 0.01 and ****P < 0.0001). (**F**) Immunohistochemical evaluation of tumor tissue (scale bars: 50 μm).

IL-23A (336 ± 74 mm^3; P < 0.05), CLSV system (602 ± 189 mm^3; P < 0.0001), and NS (893 ± 126 mm^3; P < 0.0001) groups (Figure 7C). Additionally, a lower average tumor weight was calculated in the CLSV/dual-mRNA complex group (0.20 ± 0.04 g) (Figure 7D) than in the CLSV/Bim system, CLSV/IL-23A, CLSV, and NS groups (0.59 ± 0.03 g (P < 0.01); 0.49 ± 0.08 g (P < 0.05); 0.78 ± 0.13 g (P < 0.0001); and 1.08 ± 0.22 g (P < 0.0001), respectively). In addition, as depicted in Figure 7E, the tumor inhibition rate in the CLSV/dual-mRNA complex group reached 81.41%, which was much higher than those in the CLSV/IL-23A (54.56%, P < 0.01), CLSV/Bim (45.32%, P < 0.0001), and CLSV (27.30%, P < 0.0001) groups. These results suggest that subcutaneous administration of the CLSV/dual-mRNA complex effectively suppressed the growth of CT26 subcutaneous xenografted cancer cells.

We then verified the therapeutic mechanism of the CLSV/dual-mRNA complex by immunohistochemistry and immunofluorescence. The results showed that the expression of Bim and IL-23A proteins in the CLSV/dual-mRNA complex group was similar to that in the CLSV/Bim and CLSV/IL-23A groups and much higher than that in the NS and CLSV groups, indicating that the CLSV system successfully delivered Bim and IL-23A mRNA into the tumor tissues (Figure 7F). Furthermore, the

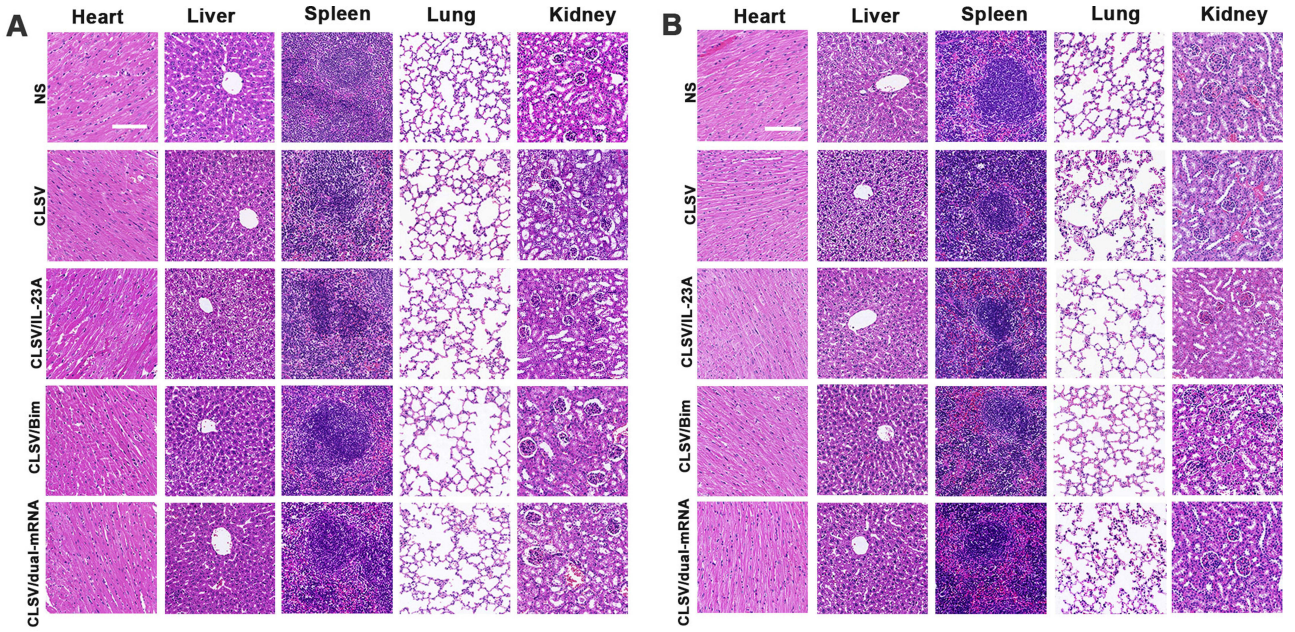

Figure 8 Hematoxylin and eosin (H&E) analysis in vivo. (**A**) H&E analysis of the main organs in the CT26 abdominal cavity metastatic model (scale bars: 100 μm). (**B**) H&E analysis of the main organs in the CT26 subcutaneous xenograft model (scale bars: 100 μm).

TUNEL assay results showed that even though the CLSV/Bim and CLSV/IL-23 groups retained an apoptotic effect, the apoptotic level of tumor cells remained higher following treatment with the CLSV/dual-mRNA complex (Figure 7F). Moreover, compared with other groups, the CD31 staining indicated an obvious reduction in microvessel density in the CLSV/dual-mRNA complex treatment group, suggesting an anti-angiogenesis effect of the CLSV/dual-mRNA complex. Additionally, similar to the CLSV/Bim group, strong positive signals of caspase-9 and caspase-3 proteins were observed in tumor sections of the CLSV/dual-mRNA complex group, indicating a significant induction of apoptosis (Figure 7F).

The CLSV/dual-mRNA complex was also found to enhance immune cell infiltration. Similar to the CLSV/IL-23A group, we noted an increase in the levels of CD4 and TNF-α markers after treatment with the CLSV/dual-mRNA complex, demonstrating its ability to activate and recruit immune cells (Figure 7F). These results collectively indicate the activation of immune responses during treatment with the CLSV/dual-mRNA complex (Figure 7F). Furthermore, it is noteworthy that there were no serious adverse effects or significant pathological changes in the major organs of treated mice in the CT26 abdominal cavity metastatic model and subcutaneous xenograft model, suggesting that intratumoral injection of the CLSV/dual-mRNA complex is safe in vivo (Figure 8A and B). Additionally, there were no significant changes or toxicity in the blood circulation, with respect to WBC, Lymph, MON, Gran, LTT, RBC, HGB, MCHC, HCT, RDW, PCT, MCV, MPV, PDW, UREA, CREA, UA, ALT, and AST (Figure 9). These results indicate that CLSV effectively transmitted Bim and IL-23A mRNAs, not only stimulating immunity but also inducing apoptosis and anti-angiogenesis to effectively inhibit the growth of CT26 tumor metastasis.

Discussion

Cancer is a complex disease associated with multiple genetic factors and gene mutations.[29] The dual-gene delivery strategy maximizes the therapeutic effect by delivering genes with different functions and has great potential in cancer treatment.[30,31] The primary challenges in dual-gene delivery include ensuring the efficient conveyance of both genes and safeguarding the binding and stability of nucleic acid molecules of varying lengths. Overcoming these hurdles primarily centers on delivery vectors. In recent years, some researchers have attempted to develop different non-viral vectors to achieve dual-gene therapy in tumors. Indeed, Wu et al designed a multivalent amphiphilic peptide dendrimer (H-Cys-SH) 2-lys-Glu(G2)-Obzl to deliver hTERT and TRF2 siRNA to treat non-small-cell lung cancer.[32] Moreover, Feng et al constructed a targeting dual-gene delivery system consisting of cationic polymer polylysine grafted with arginine protected by tosyl group (PLL-RT) and hyaluronic acid to load

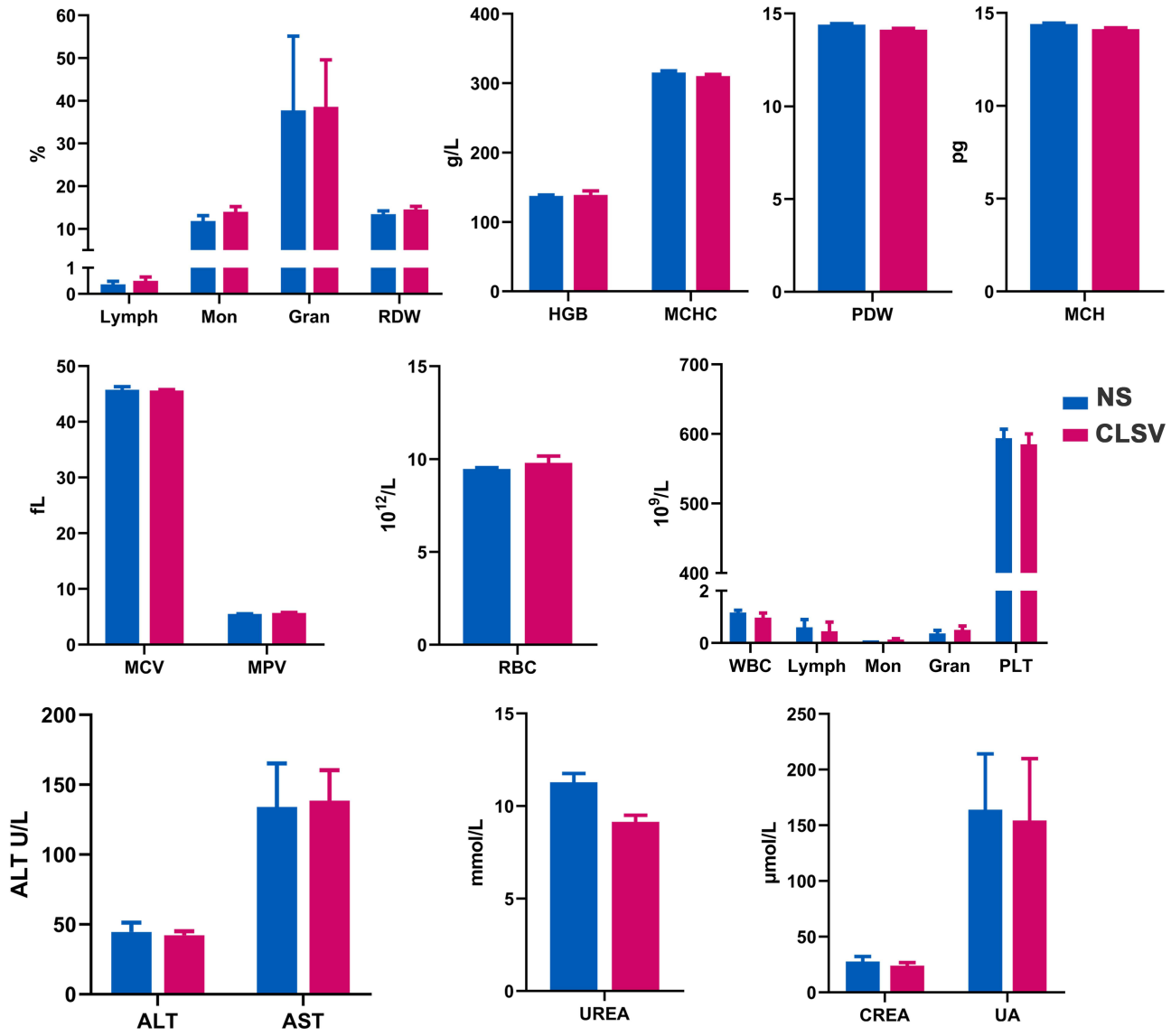

Figure 9 Blood routine analysis of mice after intravenous injection of CLSV nanoparticles.

*p*shVEGF-A and *p*shPD-L1 against murine melanoma.[33] Liu et al constructed DAL-LNP to co-deliver IL-12 and IL-27 mRNA complexes to treat B10F27 melanoma tumors.[34] Although these researchers successfully achieved dual-gene delivery and showed better therapeutic effects than a single gene, the vector composition they employed was often more complex to achieve dual-gene delivery. Even if the delivery of two mRNAs was achieved, there have been few studies on the realization of dual-mRNA delivery. In this study, we designed a novel non-viral vector with simple components and high delivery efficiency to achieve dual-mRNA delivery. Based on the DMP obtained in our previous studies, we combined DMP-mal-Lysate with new CPPs to form a dual-mRNA delivery system termed CLSV. The CLSV system could efficiently deliver two mRNAs simultaneously, with transfection efficiency of EGFP and mCherry mRNA reaching 69% and 60% in CT26 cells, respectively. Meanwhile, the CLSV system could introduce mRNA into cells through fossa protein-mediated endocytosis to achieve co-delivery of double mRNA molecules. In vitro, Bim and IL-23 mRNA could be delivered simultaneously to CT26 cells to play their respective roles. In vivo, CLSV/dual-mRNA complex showed potent anti-cancer effects in CT26 models, surpassing those achieved by single-gene delivery. One reason for these favorable results was that DMP, the main skeleton of CLSV, was a self-assembled amphiphilic micelle with small particles and a uniform charge distribution on the outer surface. Previous studies have shown that DMP could stably bind to mRNA and ensure that mRNA was not degraded during transport. Benefiting from its self-assembly structure, the system-

maintained flexibility, enabling the accommodation of diverse mRNA lengths and folded configurations. In addition, on the basis of the advantage of the existing DMP skeleton in mRNA delivery, we introduced modifications involving CPP to maximize the cell penetration capacity of this delivery system and significantly improve its mRNA delivery efficiency. In terms of the design of CPPs, we selected TAT and iRGD sequences,[35,36] two representative cellular penetrating peptides, to be connected in series instead of the CPPs modification strategy, which is coupled with the carrier to reduce the influence of steric hindrance brought by CPPs. Moreover, the covalent connection through the Michael addition reaction not only increases the stability of the connection of CPPs and performs its function, but may also facilitate the spread of CPPs on the surface of nanoparticles, further avoiding the steric hindrance introduced by modification. In the selected CPPs, the TAT peptide, as a cationic peptide, is rich in multiple arginine residues, which overcomes the possibility of the positive charge effect of the delivery carrier being reduced due to CPP modification.[37] Based on this, to further expand the function of DMP, we explored the possibility of additional delivery of tumor cell lysates into the DMP skeleton. While lacking a distinct internal cavity similar to liposomes, there were tiny gaps due to the arrangement and repulsive effects of molecules in the micelle self-assembly process, which offered the possibility of accommodating tumor lysates. In addition, owing to its self-assembly structure, the DMP skeleton had certain deformation and encapsulation capabilities, facilitating cargo wrapping from inside and outside, thus enabling the concurrent conveyance of both mRNA and tumor cell lysates within a single carrier.

Stimulating the organism's immune response is a pivotal strategy in cancer treatment, and the use of tumor cell lysates as a potential immunotherapeutic approach has shown promise in the field of tumor therapy. However, the challenge lies in harnessing and maximizing the immune-stimulatory effects of lysates owing to their inherent complexity. In recent years, researchers have made many attempts to apply tumor cell lysates to explore their potential in therapy. Indeed, Kawahara et al reported that the combination (BLP) of CT26 tumor lysate, baculovirus, and a cytotoxic T-cell epitope peptide could provide strong anti-tumor immunity to suppress tumor growth, which was attributed to the function of CD4(+) T cells stimulated with tumor lysate.[38] Moreover, Tang et al used tumor lysate and an interleukin-18 gene-modified DC vaccine to treat pancreatic cancer.[39] Shi et al developed surface-modified mannose chitosan-based nanoparticles (MAN-CTS NPs) loaded with tumor cell lysate (TCL) produced by B16 melanoma cells to improve the efficacy of anti-tumor immune responses compared with TCL alone.[40] The aforementioned studies have successfully realized the use of tumor lysate for tumor therapy, but the immune stimulation effect in the application process remains unsatisfactory, and there have been few instances whereby delivery systems have been used to deliver tumor cell lysate for tumor therapy. In our study, we wrapped CT26 tumor cell lysate into the DMP skeleton to form the CLSV system and proved that this system could not only deliver double mRNA molecules simultaneously but also effectively encapsulate tumor cell lysate to play its immune-stimulating function. The results showed that the prepared CLSV system could be absorbed by BMDCs and promote its maturity. In vivo, we analyzed immune cells in the LNs and spleens of mice at different time points after immunostimulation with DMP-CPPs, tumor cell lysate, and CLSV, and the results showed that the prepared CLSV could recruit immune cells to a greater extent. The results of animal experiments showed that the CLSV system could inhibit tumor growth and had anti-cancer potential. One of the reasons for these desirable results is that we used cationic nanoparticles to deliver tumor cell lysates, potentially offering multifaceted advantages. Previous studies have demonstrated the slow drug-releasing capabilities of DMP, suggesting that the constructed CLSV system could slow the release of tumor cell lysates.[41] Even though the composition of tumor cell lysate was complex, the positive charge of CLSV could not only slow the dissociation and diffusion of tumor cell lysate from the surface of the nanoparticle through the effect of electrostatic adsorption but could also delay the antigen release rate given that DMP wrapped tumor cell lysate such that it needed to be dissociated layer-by-layer to be released. This controlled release promoted a more uniform dispersion and stabilization of the complex components in the lysate, thereby preventing the rapid clearance of these antigens and extending their exposure to the immune system. In addition, Sheppard et al proved that polyethyleneimine, as a cationic nanocarrier, could further enhance antigen uptake and serve as a potent mucosal adjuvant.[42] As well as polyethyleneimine, appropriate size and surface properties of cationic nanoparticles based on the CLSV skeleton could extend the circulation time and effectively deliver tumor cell lysates to antigen-presenting cells, such as DCs, which is critical for initiating and directing the immune response against cancer. Furthermore, studies have shown that cationic nanoparticles can stimulate the immune system. For instance, Kedmi et al proved that positively charged lipid nanoparticles could induce Th1 cytokine expression and activate the immune system.[43] As expected, this immune-stimulatory effect of CLSV could

further potentiate the immune response triggered by tumor cell lysates; thus, the combination of CLSV, as cationic nanocarriers, and tumor cell lysates enhanced immune system reinforcement.

Conclusions

In this study, we designed a composite nanodelivery system capable of simultaneously delivering Bim-coding and IL-23A-coding mRNAs for treating colon cancer. By modifying its surface with fused CPPs and encapsulating the CT26 tumor cell lysate, the system achieved the dual purpose of simultaneously delivering Bim and IL-23A mRNAs and activating the immune response. The results demonstrated that CLSV could efficiently and safely deliver Bim and IL-23A mRNAs into CT26 cells. The prepared CLSV/dual-mRNA complex exhibited significant anti-cancer effects in subcutaneous and intraperitoneal colon cancer models. Therefore, CLSV represents an ideal dual-functional system that not only encapsulates CT26 tumor cell lysate but also delivers double mRNA molecules to treat tumors in multiple ways.

Data Sharing Statement

The authors declare that the data supporting the findings of this study are available within the paper or from the corresponding authors upon request.

Acknowledgments

This work was supported by Medico-Engineering Cooperation Funds from university of Electronic Science and Technology of China (No. ZYGX2021YGLH225), the Key Research Program of Science and Technology Department of Sichuan Province (2023YFS0165, 23NSFJQ0104) and the Science Foundation of Chengdu (2022-YF05-01793-SN).

Disclosure

The authors declare that they have no conflicts of interest in this work.

References

1. Siegel RL, Miller KD, Fuchs HE, Jemal A. Cancer Statistics, 2021. *Ca a Cancer J Clinicians*. 2021;71(1):7–33. doi:10.3322/caac.21654
2. Herrmann J. Adverse cardiac effects of cancer therapies: cardiotoxicity and arrhythmia. *Nat Rev Cardiol*. 2020;17(8):474–502. doi:10.1038/s41569-020-0348-1
3. Liu C, Shi Q, Huang X, Koo S, Kong N, Tao W. mRNA-based cancer therapeutics. *Nat Rev Cancer*. 2023;23(8):526–543. doi:10.1038/s41568-023-00586-2
4. Qiu M, Li Y, Bloomer H, Xu Q. Developing biodegradable lipid nanoparticles for intracellular mRNA delivery and genome editing. *Acc Chem Res*. 2021;54(21):4001–4011. doi:10.1021/acs.accounts.1c00500
5. Beck JD, Reidenbach D, Salomon N, et al. mRNA therapeutics in cancer immunotherapy. *Mol Cancer*. 2021;20(1):69. doi:10.1186/s12943-021-01348-0
6. Oliver SE, Gargano JW, Marin M, et al. The advisory committee on immunization practices' interim recommendation for use of Pfizer-BioNTech COVID-19 vaccine - United States, December 2020. *MMWR Morb Mortal Wkly Rep*. 2020;69(50):1922–1924. doi:10.15585/mmwr.mm6950e2
7. Corbett KS, Flynn B, Foulds KE, et al. Evaluation of the mRNA-1273 Vaccine against SARS-CoV-2 in nonhuman primates. *New Engl J Med*. 2020;383(16):1544–1555. doi:10.1056/NEJMoa2024671
8. Gao B, Wang X, Wang M, et al. From single to a dual-gene delivery nanosystem: coordinated expression matters for boosting the neovascularization in vivo. *Biomater Sci*. 2020;8(8):2318–2328. doi:10.1039/c9bm02000d
9. Jiang L, Park JS, Yin L, et al. Dual mRNA therapy restores metabolic function in long-term studies in mice with propionic acidemia. *Nat Commun*. 2020;11(1):5339. doi:10.1038/s41467-020-19156-3
10. Kowalski PS, Rudra A, Miao L, Anderson DG. Delivering the messenger: advances in technologies for therapeutic mRNA delivery. *Mol Therap*. 2019;27(4):710–728. doi:10.1016/j.ymthe.2019.02.012
11. Futaki S, Nakase I. Cell-surface interactions on arginine-rich cell-penetrating peptides allow for multiplex modes of internalization. *Acc Chem Res*. 2017;50(10):2449–2456. doi:10.1021/acs.accounts.7b00221
12. Guidotti G, Brambilla L, Rossi D. Cell-penetrating peptides: from basic research to clinics. *Trends Pharmacol Sci*. 2017;38(4):406–424. doi:10.1016/j.tips.2017.01.003
13. Madani F, Lindberg S, Langel U, Futaki S, Gräslund A. Mechanisms of cellular uptake of cell-penetrating peptides. *J Biophy*. 2011;2011:414729. doi:10.1155/2011/414729
14. Boisguérin P, Deshayes S, Gait MJ, et al. Delivery of therapeutic oligonucleotides with cell penetrating peptides. *Adv Drug Delivery Rev*. 2015;87:52–67. doi:10.1016/j.addr.2015.02.008
15. Zen M, Canova M, Campana C, et al. The kaleidoscope of glucorticoid effects on immune system. *Autoimmunity Rev*. 2011;10(6):305–310. doi:10.1016/j.autrev.2010.11.009
16. Chaurio RA, Janko C, Muñoz LE, Frey B, Herrmann M, Gaipl US. Phospholipids: key players in apoptosis and immune regulation. *Molecules*. 2009;14(12):4892–4914. doi:10.3390/molecules14124892
17. Garcia-Garijo A, Fajardo CA, Gros A. Determinants for neoantigen identification. *Front Immunol*. 2019;10:1392. doi:10.3389/fimmu.2019.01392

18. Zalba S, Ten Hagen TL. Cell membrane modulation as adjuvant in cancer therapy. *Cancer Treat Rev*. 2017;52:48–57. doi:10.1016/j.ctrv.2016.10.008
19. Aikins ME, Xu C, Moon JJ. Engineered nanoparticles for cancer vaccination and immunotherapy. *Acc Chem Res*. 2020;53(10):2094–2105. doi:10.1021/acs.accounts.0c00456
20. Salewski I, Gladbach YS, Kuntoff S, et al. In vivo vaccination with cell line-derived whole tumor lysates: neoantigen quality, not quantity matters. *J Transl Med*. 2020;18(1):402. doi:10.1186/s12967-020-02570-y
21. Kim JH, Lee Y, Bae YS, et al. Phase I/II study of immunotherapy using autologous tumor lysate-pulsed dendritic cells in patients with metastatic renal cell carcinoma. *Clin Immunol*. 2007;125(3):257–267. doi:10.1016/j.clim.2007.07.014
22. Gao Y, Men K, Pan C, et al. Functionalized DMP-039 hybrid nanoparticle as a novel mRNA vector for efficient cancer suicide gene therapy. *Int j Nanomed*. 2021;16:5211–5232. doi:10.2147/ijn.S319092
23. Li J, Men K, Gao Y, et al. Single micelle vectors based on lipid/block copolymer compositions as mRNA Formulations for efficient cancer immunogene therapy. *Mol Pharmaceut*. 2021;18(11):4029–4045. doi:10.1021/acs.molpharmaceut.1c00461
24. Zhu R, Li L, Nguyen B, et al. FLT3 tyrosine kinase inhibitors synergize with BCL-2 inhibition to eliminate FLT3/ITD acute leukemia cells through BIM activation. *Signal Transduc Target Therap*. 2021;6(1):186. doi:10.1038/s41392-021-00578-4
25. Schinocca C, Rizzo C, Fasano S, et al. Role of the IL-23/IL-17 pathway in rheumatic diseases: an overview. *Front Immunol*. 2021;12:637829. doi:10.3389/fimmu.2021.637829
26. Men K, Huang R, Zhang X, et al. Local and systemic delivery of interleukin-12 gene by cationic micelles for cancer immunogene therapy. *J Biomed Nanotechnol*. 2018;14(10):1719–1730. doi:10.1166/jbn.2018.2593
27. Perez AP, Cosaka ML, Romero EL, Morilla MJ. Uptake and intracellular traffic of siRNA dendriplexes in glioblastoma cells and macrophages. *Int j Nanomed*. 2011;6:2715–2728. doi:10.2147/ijn.S25235
28. Lei S, Zhang X, Men K, et al. Efficient colorectal cancer gene therapy with IL-15 mRNA nanoformulation. *Mol Pharmaceut*. 2020;17(9):3378–3391. doi:10.1021/acs.molpharmaceut.0c00451
29. Sugimura T, Terada M, Yokota J, Hirohashi S, Wakabayashi K. Multiple genetic alterations in human carcinogenesis. *Environ Health Perspect*. 1992;98:5–12. doi:10.1289/ehp.92985
30. Lei S, Gao Y, Li J, et al. Dual-RNA controlled delivery system inhibited tumor growth by apoptosis induction and TME activation. *J Cont Rel*. 2022;344:97–112. doi:10.1016/j.jconrel.2022.02.022
31. Wang P, Logeart-Avramoglou D, Petite H, et al. Co-delivery of NS1 and BMP2 mRNAs to murine pluripotent stem cells leads to enhanced BMP-2 expression and osteogenic differentiation. *Acta Biomater*. 2020;108:337–346. doi:10.1016/j.actbio.2020.03.045
32. Wu Y, Zhong D, Li Y, et al. A tumor-activatable peptide supramolecular nanoplatform for the delivery of dual-gene targeted siRNAs for drug-resistant cancer treatment. *Nanoscale*. 2021;13(9):4887–4898. doi:10.1039/d0nr08487e
33. Feng Y, Wu J, Chen J, et al. Targeting dual gene delivery nanoparticles overcomes immune checkpoint blockade induced adaptive resistance and regulates tumor microenvironment for improved tumor immunotherapy. *Nano Today*. 2021;38:101194. doi:10.1016/j.nantod.2021.101194
34. Liu JQ, Zhang C, Zhang X, et al. Intratumoral delivery of IL-12 and IL-27 mRNA using lipid nanoparticles for cancer immunotherapy. *J Cont Rel*. 2022;345:306–313. doi:10.1016/j.jconrel.2022.03.021
35. Tietz O, Cortezon-Tamarit F, Chalk R, Able S, Vallis KA. Tricyclic cell-penetrating peptides for efficient delivery of functional antibodies into cancer cells. *Nature Chem*. 2022;14(3):284–293. doi:10.1038/s41557-021-00866-0
36. Wan WJ, Huang G, Wang Y, et al. Coadministration of iRGD peptide with ROS-sensitive nanoparticles co-delivering siFGL1 and siPD-L1 enhanced tumor immunotherapy. *Acta Biomater*. 2021;136:473–484. doi:10.1016/j.actbio.2021.09.040
37. Stanzl EG, Trantow BM, Vargas JR, Wender PA. Fifteen years of cell-penetrating, guanidinium-rich molecular transporters: basic science, research tools, and clinical applications. *Acc Chem Res*. 2013;46(12):2944–2954. doi:10.1021/ar4000554
38. Kawahara M, Takaku H. A tumor lysate is an effective vaccine antigen for the stimulation of CD4+ T-cell function and subsequent induction of antitumor immunity mediated by CD8+ T cells. *Cancer Biol Ther*. 2015;16(11):1616–1625. doi:10.1080/15384047.2015.1078027
39. Tang ZH, Qiu WH, Wu GS, Yang XP, Zou SQ, Qiu FZ. The immunotherapeutic effect of dendritic cells vaccine modified with interleukin-18 gene and tumor cell lysate on mice with pancreatic carcinoma. *World J Gastroenterol*. 2002;8(5):908–912. doi:10.3748/wjg.v8.i5.908
40. Shi GN, Zhang CN, Xu R, et al. Enhanced antitumor immunity by targeting dendritic cells with tumor cell lysate-loaded chitosan nanoparticles vaccine. *Biomaterials*. 2017;113:191–202. doi:10.1016/j.biomaterials.2016.10.047
41. Men K, Liu W, Li L, et al. Delivering instilled hydrophobic drug to the bladder by a cationic nanoparticle and thermo-sensitive hydrogel composite system. *Nanoscale*. 2012;4(20):6425–6433. doi:10.1039/c2nr31592k
42. Sheppard NC, Brinckmann SA, Gartlan KH, et al. Polyethyleneimine is a potent systemic adjuvant for glycoprotein antigens. *Internat Immunol*. 2014;26(10):531–538. doi:10.1093/intimm/dxu055
43. Kedmi R, Ben-Arie N, Peer D. The systemic toxicity of positively charged lipid nanoparticles and the role of Toll-like receptor 4 in immune activation. *Biomaterials*. 2010;31(26):6867–6875. doi:10.1016/j.biomaterials.2010.05.027